2017

Functional Specialization of Cellulose Synthase Isoforms in a Moss Shows Parallels with Seed Plants

Joanna H. Norris
University of Rhode Island, jnorris@uri.edu

Xingxing Li
University of Rhode Island

See next page for additional authors

Citation/Publisher Attribution
Norris, J. H., Li, X., Huang, S., Van de Meene, A. M.L., Tran, M. L., Killeavy, E., Chaves, A. M.,...Roberts, A. W. (2017). Functional Specialization of Cellulose Synthase Isoforms in a Moss Shows Parallels with Seed Plants. *Plant Physiology, 175*, 210-222. doi: 10.1104/pp.17.00885
Available at: https://doi.org/10.1104/pp.17.00885

Short title: CESA functional specialization in *Physcomitrella*

Corresponding author:

Alison W. Roberts, Department of Biological Sciences, University of Rhode Island, 120 Flagg Road, Kingston RI 02881 USA, email: aroberts@uri.edu, telephone: 401-874-4098, ORCID ID: 0000-0002-7775-5589

Title: Functional specialization of cellulose synthase isoforms in a moss shows parallels with seed plants

Joanna H. Norris[a], Xingxing Li[a], Shixin Huang[b], Allison M.L. Van de Meene[c], Mai L. Tran[a], Erin Killeavy[a], Arielle M. Chaves[a], Bailey Mallon[a], Danielle Mercure[a], Hwei-Ting Tan[d], Rachel A. Burton[d], Monika S. Doblin[c], Seong H. Kim[b], Alison W. Roberts[a]

[a]Department of Biological Sciences, University of Rhode Island, Kingston RI 02881, USA

[b]Department of Chemical Engineering, The Pennsylvania State University, University Park, PA 16802, USA

[c]ARC Centre of Excellence in Plant Cell Walls, Plant Cell Biology Research Centre, School of BioSciences, The University of Melbourne, Victoria 3010, Australia.

[d]ARC Centre of Excellence in Plant Cell Walls, School of Agriculture, Food and Wine, University of Adelaide, Waite Campus, Glen Osmond, South Australia 5064, Australia

One sentence summary: Regulatory uncoupling of primary and secondary cellulose synthases occurred independently in mosses and seed plants, and is associated with convergent evolution of secondary wall structure.

List of author contributions: J.H.N. and A.W.R. conceived the project, and supervised and performed experiments; X.L., S.H., A.M.L.VdM., and M.L.T. designed and performed experiments, and analyzed the data; A.M.C., E.K., B.M., D.M. and H-T.T. performed experiments; S.H.K. supervised experiments; A.W.R. wrote the manuscript with contributions from J.H.N., S.H., A.M.L.V., S.H.K., R.A.B. and M.S.D. All authors read and approved the manuscript.

Funding information: This work was supported primarily by National Science Foundation Award IOS-1257047. Analysis of mutants by SFG spectroscopy was supported as part of The Center for LignoCellulose Structure and Formation, an Energy Frontier Research Center funded by the U.S. Department of Energy, Office of Science, Office of Basic Energy Sciences under Award Number DE-

SC0001090. CBM3a affinity cytochemistry and freeze substitution transmission electron microscopy were supported by the Australian Research Council Centre for Excellence in Plant Cell Walls Grant CE1101007. High pressure freezing and transmission electron microscopy was undertaken at the Melbourne Advanced Microscopy Facility at the Bio21 Institute and the Biosciences Microscopy Unit at The University of Melbourne. DNA sequencing and qPCR were conducted using the Rhode Island Genomics and Sequencing Center, a Rhode Island NSF EPSCoR research facility, supported in part by the National Science Foundation EPSCoR Cooperative Agreement EPS-1004057.

Present addresses: BM, Neuroimaging Research Branch, National Institutes of Health, Baltimore, MD 21224, USA; DM, Pfizer Inc., Groton, CT 06340, USA; H-T Tan, Centre for Tropical Crops and Biocommodities, Queensland University of Technology, Brisbane, QLD 4000, Australia.

Corresponding author email: aroberts@uri.edu

Abstract

The secondary cell walls of tracheary elements and fibers are rich in cellulose microfibrils that are helically oriented and laterally aggregated. Support cells within the leaf midribs of mosses deposit cellulose-rich secondary cell walls, but their biosynthesis and microfibril organization have not been examined. Although the *Cellulose Synthase* (*CESA*) gene families of mosses and seed plants diversified independently, *CESA* knockout analysis in the moss *Physcomitrella patens* revealed parallels in CESA functional specialization of Arabidopsis and *P. patens*, with roles for both sub-functionalization and neo-functionalization. The similarities include regulatory uncoupling of the CESAs that synthesize primary and secondary cell walls, a requirement for two or more functionally distinct CESA isoforms for secondary cell wall synthesis, interchangeability of some primary and secondary CESAs, and some CESA redundancy. The cellulose-deficient midribs of *ppcesa3/8* knockouts provided negative controls for structural characterization of stereid secondary cell walls in wild type *P. patens*. Sum frequency generation spectra collected from midribs were consistent with cellulose microfibril aggregation, and polarization microscopy revealed helical microfibril orientation only in wild type leaves. Thus, stereid secondary walls are structurally distinct from primary cell walls, and they share structural characteristics with the secondary walls of tracheary elements and fibers. We propose a mechanism for convergent evolution of secondary walls in which deposition of aggregated and helically oriented microfibrils is coupled to rapid and highly localized cellulose synthesis enabled by regulatory uncoupling from primary wall synthesis.

Introduction

In vascular plants, cellulose is a major component of both primary cell walls that are deposited during cell expansion and secondary cell walls that are deposited after expansion has ceased (Carpita and McCann 2000). Secondary cell walls of water-conducting tracheary elements and supportive fibers are rich in cellulose with microfibrils arranged in helices that vary in angle according to developmental stage and environmental conditions (Barnett and Bonham 2004). Secondary cell wall microfibrils are also more aggregated than those of primary cell walls (Donaldson 2007; Fernandes et al. 2011; Thomas et al. 2014). Recently, Sum Frequency Generation (SFG) spectroscopy has been used to compare the mesoscale structure of cellulose microfibrils in primary and secondary cell walls. Both high cellulose content and microfibril aggregation contribute to a strong secondary cell wall signature in SFG spectra of mature angiosperm tissues (Barnette et al. 2012; Lee et al. 2014; Park et al. 2013).

Cellulose microfibrils are synthesized by cellulose synthase (CESA) proteins that function together as cellulose synthesis complexes (CSCs) in the plasma membrane (Delmer 1999; Kimura et al. 1999).

Recent analyses of CSC and microfibril structure indicate that the rosette CSCs of land plants most likely contain 18 CESA subunits (Fernandes et al. 2011; Jarvis 2013; Newman et al. 2013; Nixon et al. 2016; Oehme et al. 2015; Thomas et al. 2014; Vandavasi et al. 2016) in a 1:1:1 ratio (Gonneau et al. 2014; Hill et al. 2014). Seed plants have six phylogenetic and functional classes of CESA proteins, three required for primary cell wall synthesis (Desprez et al. 2007; Persson et al. 2007) and three required for synthesis of the lignified secondary cell walls of tracheary elements and fibers (Taylor et al. 2003). Mutation of any of the secondary CESAs results in a distinctive irregular xylem phenotype characterized by collapsed xylem tracheary elements and weak stems (Taylor et al. 2004). The secondary cell wall CESAs of Arabidopsis are regulated by master regulator NAC domain transcription factors that also activate genes required for the synthesis of other secondary cell wall components, such as xylan and lignin (Schuetz et al. 2013; Yang and Wang 2016; Zhong and Ye 2015).

The moss *Physcomitrella patens* (Hedw.) B. S. G. has seven *CESA* genes (Goss et al. 2012; Roberts and Bushoven 2007). Phylogenetic analysis has revealed that the *P. patens* CESAs do not cluster with the six CESA clades shared by seed plants (Roberts and Bushoven 2007). Like other mosses, *P. patens* lacks the lignified secondary cell walls that are characteristic of vascular plant tracheary elements and fibers. However, mosses do have support cells (stereids) with thick unlignifed cell walls (Kenrick and Crane 1997) and water-conducting cells (hydroids) that have thin cell walls and undergo programmed cell death like tracheary elements (Hebant 1977). Although the stereid cell walls of *P. patens* are known to contain cellulose (Berry et al. 2016), the mesoscale structure has not been examined. Only one of the seven *P. patens* CESAs has been characterized functionally. When *PpCESA5* was disrupted, gametophore buds failed to develop into leafy gametophores, instead forming irregular cell clumps. The associated disruption of cell expansion and cell division are consistent with an underlying defect in primary cell wall deposition (Goss et al. 2012). Recently it was shown that *PpCESA3* expression is regulated by the NAC transcription factor *PpVNS7*, along with thickening of stereid cell walls (Xu et al. 2014).

Here we show that PpCESA3 and PpCESA8 function in the deposition of stereid cell walls in the gametophore leaf midribs of *P. patens* and are sub-functionalized with respect to PpCESA5. We also used polarization microscopy and SFG to reveal similarities in the mesoscale organization of the microfibrils synthesized by PpCESA3 and PpCESA8 and those in the secondary cell walls of vascular plants. Finally, we propose a mechanism through which uncoupling of primary and secondary CESA regulation played a role in independent evolution of secondary cell walls with aggregated, helically arranged cellulose microfibrils in the moss and seed plant lineages.

Results

PpCESA3 and PpCESA8 function in secondary cell wall deposition

Cellulose synthase genes *PpCESA3* and *PpCESA8* were independently knocked out by homologous recombination in an effort to examine their roles in development and cell wall biosynthesis in *P. patens*. Stable antibiotic resistant lines generated by transforming wild type *P. patens* with CESA3KO or CESA8KO vectors were tested for integration of the vector and deletion of the target gene by PCR (Fig. S1). Integration was verified for five *ppcesa8*KO lines recovered from two different transformations, line 8KO5B from a transformation of the GD06 wild type line and lines 8KO4C, 8KO5C, 8KO7C and 8KO10C from a transformation of the GD11 wild type line (Fig. S1). Integration was verified for three *ppcesa3*KO lines recovered from a single transformation of GD11 and three double *ppcesa3/8*KO lines recovered from a single transformation of the *ppcesa8*KO5B line with the CESA3KO vector (Fig. S1). The GD06 and GD11 lines are from independent selfings of the same haploid wild type line, as described in Materials and Methods.

The colonies that developed from wild type and KOs consisted of protonemal filaments and leafy gametophores (Fig. 1). Whereas wild type, *ppcesa3*KO, and *ppcesa8*KO gametophores grew vertically, the gametophores on *ppcesa3*/*8*KO colonies were unable to support themselves and adopted a horizontal orientation. Superficially *ppcesa3*/*8*KO colonies appeared to produce fewer gametophores (Fig. 1), but dissection revealed similar numbers of horizontal gametophores that had been overgrown by protonemal filaments. Thus, PpCESA3 and PpCESA8 are not required for gametophore initiation or morphogenesis, but they appear to contribute to structural support.

When examined with polarized light microscopy, the wild type gametophore leaves exhibited strong cell wall birefringence in the midribs and margins (Fig. 1). In contrast, the leaves produced by *ppcesa3/8*KOs lacked strong birefringence in these cells, consistent with reduced crystalline cellulose content. The *ppcesa3*KO leaves appeared similar to wild type leaves (Fig. 1) and *ppcesa8*KO leaves had an intermediate phenotype. Staining with the fluorescent cellulose binding dye Pontamine Fast Scarlet (S4B) (Anderson et al. 2010) produced similar results with strong fluorescence in the midribs of wild type and *ppcesa3*KO leaves, weak fluorescence in *ppcesa3*/*8*KO leaves, and intermediate fluorescence in *ppcesa8*KO leaves (Fig. 1).

Cellulose Binding Module (CBM) 3a provides a third method for detecting cellulose and can be used to probe thin sections (Blake et al. 2006). In sections from fully expanded wild type leaves, the walls of the lamina cells were labeled relatively weakly with CBM3a, whereas the thickened cell walls of the central

midrib and bundle sheath cells were strongly labeled (Fig. 1). The same was true for *ppcesa3*KO leaves. However, midrib and bundle sheath cell labeling was nearly absent in *ppcesa3/8*KO and diminished in *ppcesa8*KO (Fig. 1) compared to wild type and *ppcesa3*KO. Differential interference contrast microscopy of the same sections showed enhanced contrast in wild type and *ppcesa3*KO midribs (Fig. 1). Partial cell collapse occurred during embedding in *ppcesa3/8*KO leaves (Fig. 1).

The cellulose content of the leaf midribs in wild type and single and double *ppcesa*KO mutants was quantified by measuring the intensity of S4B fluorescence. Statistical analysis confirmed that the S4B fluorescence was significantly reduced in double KOs, but not in *ppcesa3*KOs (Fig. 2). The intermediate phenotype of the *ppcesa8*KOs was confirmed and shown to be significantly different from both wild type and the double KOs (Fig. 2). Updegraff analysis showed that cellulose content of cell walls from whole *ppcesa3/8*KO gametophores (mean±S.E. of three genetic lines = 33.8±0.034%) was reduced significantly ($p = 0.004$) compared to wild type (GD06, mean±S.E. of three independent cultures = 60.1±0.030%).

To confirm that the observed *ppcesa3/8*KO phenotype was due to the absence of PpCESA3 and PpCESA8, the selection cassette was removed from *ppcesa3/8*KO-86 by Cre-mediated recombination of flanking *lox-p* sites (Vidali et al. 2010) to allow transformation with vectors that drive expression of PpCESA3 or PpCESA8 with their native promoters (Fig. S2). Stable antibiotic resistant lines selected for the presence of numerous erect gametophores were examined with polarization microscopy (Fig. S2). For the transformation with *proCESA8::CESA8*, 13 lines were examined, 6 of these had strong midrib birefringence, and the first 3 were used for further analysis. For the transformation with *proCESA3::CESA3*, the first three lines examined had strong midrib birefringence and were used for further analysis. S4B staining confirmed that expression of PpCESA8 or PpCESA3 rescued the defects in cellulose deposition in the leaf midribs of the double *ppcesa3/8*KO (Fig. 2). Lines from the transformation with *proCESA8::CESA8* were expected to be restored to the wild type phenotype because *ppcesa3*KO, which also expresses *PpCESA8* under control of the *PpCESA8* promoter, showed no defects in cellulose deposition in the leaf midrib. All three *proCESA8::CESA8* lines had significantly stronger S4B fluorescence than *ppcesa8*KO. This demonstrates substantial restoration of the phenotype, although fluorescence was still significantly weaker than the wild type (Fig. 2). Two lines from a transformation with *proCESA3::CESA3* (3R29 and 3R52) were not significantly different from *ppcesa8*KO-5B, which is expected since they both lack *PpCESA8* and express *PpCESA3* under control of the *PpCESA3* promoter. In the third line (3R45) fluorescence was restored to wild type levels (Fig. 2). Y-axis scales differ between experiments due to the use of different exposure time settings.

Secondary cell wall microfibrils are helically oriented and laterally aggregated

A first order retardation plate was used with polarized light microscopy to determine the optical sign, and thus the cellulose microfibril orientation, of wild type and *ppcesa3/8KO* midrib cell walls (Fig. 3). In mature wild type leaves, the larger bundle sheath-like cells that surround the central stereids showed blue addition colors when oriented parallel to the major axis of the plate and yellow subtraction colors when oriented perpendicular to the major axis (Fig. 3), indicating that the net orientation of positively birefringent cellulose microfibrils is longitudinal. In contrast, the walls of the smaller central stereids were colorless when oriented parallel or perpendicular to the major axis (Fig. 3). However, when oriented at 45^{o} to the retardation plate, these cells showed alternating bands of blue and yellow (Fig. 3), indicating that the microfibrils in their walls are helical with an angle near 45^{o}. The central midrib cells of developing wild type leaves showed a transition from colorless to blue to yellow along the apical to basal developmental gradient when the midrib was oriented parallel to the major axis of the plate (Fig. 3). This indicates that the microfibril orientation changes from transverse to longitudinal and then to helical as the cells mature. In contrast, the central midrib stereids of mature *ppcesa3/8KO* leaves had blue addition colors when oriented parallel to the major axis, yellow subtraction colors when oriented perpendicular to the major axis, and no interference color when oriented at 45^{o} to the retardation plate indicating that microfibrils are longitudinal, rather than helical. Developing *ppcesa3/8KO* leaves had no longitudinal gradient in interference colors (Fig. 3).

The walls of midrib cells were examined by transmission electron microscopy in ultrathin sections of chemically fixed gametophore leaves. Despite the reduced cellulose content detected by other means, the walls of midrib cells were thickened compared to walls of adjacent lamina cells in all *ppcesa*KOs, as well as wild type leaves (Fig. 4). When we attempted to prepare specimens by high pressure freezing and freeze-substitution, the leaves fractured in a plane parallel to the midrib. This resulted in a loss of midrib cells and precluded examination of midrib cell walls in these specimens. We were able to examine the lamina and margin cells of freeze-substituted leaves in wild type and two lines of each mutant. The walls of these cells appeared similar between wild type, and single and double *ppcesa*KOs (Fig. S3). However, measurements revealed that lamina cell external walls, i.e. those facing the external environment, were thinner in *ppcesa*KOs (Fig. S4).

The mesoscale organization of cellulose in the midribs of wild type, *ppcesa3/8*KO, and *ppcesa8*KO leaves was examined using a broadband SFG microscope (Lee et al. 2016). Because it detects only non-centrosymmetric ordering of functional groups, SFG provides a means of analyzing cellulose in intact cell walls with relatively little interference from matrix components (Barnette et al. 2011). For each genotype,

full SFG spectra collected from three different locations along the midribs of each of three different leaves were averaged (Fig. 5). The sampling depth of the SFG microscope for cellulosic samples is 20-25 μm (Lee et al. 2016). Given that the thickness of turgid leaves is about 50-60 μm at the midrib and that they likely collapse to less than half their thickness when dried, we conclude that most of the leaf thickness contributes to the SFG signal. In spectra collected from the wild type, a strong peak at 2944 cm^{-1}, which is characteristic of secondary cell walls, was observed in the CH/CH_2 stretch region along with a 3320 cm^{-1} peak in the OH stretch region. In contrast, the spectra collected from *ppcesa3/8*KO and *ppcesa8*KO midribs had weaker peak intensity overall with a broad CH/CH_2 stretch peak centered around 2910 cm^{-1}. Compared to *ppcesa3/8*KO, the spectra from *ppcesa8*KO midribs had a weak signal at 2963 cm^{-1} that was absent in spectra collected from *ppcesa3/8*KO midribs. A scan across a wild type leaf shows that the 2944 cm^{-1} signal is associated with the midrib and was not observed in the cells of the lamina (Fig. 5). Equivalent scans of *ppcesa3/8*KO and *ppcesa8*KO leaves confirm the absence of a strong 2944 cm^{-1} peak from the midribs of these mutants (Fig. 5).

PpCESA proteins are functionally specialized

Based on the *ppcesa3*KO, *ppcesa8*KO, and *ppcesa3/8*KO phenotypes, PpCESA3 and PpCESA8 appear to be partially redundant. To determine whether the relative strengths of these phenotypes are related to gene expression levels, we used reverse transcription quantitative PCR to measure the expression of *PpCESA3* and *PpCESA8* in the wild type and mutants. In the *ppcesa3*KOs, *PpCESA8* was significantly upregulated compared to wild type (Fig. 6), providing a possible explanation for the lack of a mutant phenotype in these lines. In contrast, *PpCESA3* was not significantly upregulated in the *ppcesa8*KOs compared to wild type, potentially explaining the intermediate phenotype in these mutants.

*ppcesa3*KOs, *ppcesa8*KOs and *pp*cesa*3/8*KOs were tested for changes in rhizoid and caulonema development to determine whether developmental defects were restricted to the gametophores. When cultured on medium containing auxin, all lines produced the expected leafless gametophores with numerous rhizoids (Fig. S5), indicating no defects in rhizoid development in any of the KOs. Caulonema produced by colonies grown in the dark on vertically oriented plates were all negatively gravitropic (Fig. S6). Although appearance of the caulonema varied among experiments, those produced by KOs were always similar to control wild type within the same experiment. Caulonemal length was not significantly different between *ppcesa3/8*KOs and wild type (Table 1).

To determine whether other PpCESAs are functionally interchangeable with PpCESA3 and PpCESA8, we tested for rescue of *ppcesa3/8*KO-86lox by various *PpCESA*s driven by the *PpCESA8* promoter. Polarization microscopy screening of at least 21 and up to 27 stably transformed lines for each vector

revealed little or no midrib birefringence for the *proCESA8::CESA4*, *proCESA8::CESA7* and *proCESA8::CESA10* lines and moderate to strong midrib birefringence for 92% and 78% of the *proCESA8::CESA3* and *proCESA8::CESA5* lines, respectively. Quantitative analysis of S4B staining (Fig. 7) confirmed that the *ppcesa3/8*KO phenotype was partially rescued by *proCESA8::CESA3* (3 out of 3 lines) and *proCESA8::CESA5* (2 out of 3 lines) as we observed for *proCESA8::CESA8* (Fig. 2). However, the *proCESA8::CESA4*, *proCESA8::CESA7* and *proCESA8::CESA10* vectors showed no rescue (Fig. 7). Western blot analysis confirmed that PpCESA proteins were expressed in all lines except *proCESA8::CESA4*-11 and *proCESA8::CESA5*-7 (Fig. S7). PpCESA6 differs from PpCESA7 by only 2 amino acids and was not tested. Although expressed with the same promoter, protein accumulation varies among the different transgenic lines (Fig. S7). Similar differences in protein accumulation may also explain variation in the extent of rescue by the *proCESA3::CESA3* and *proCESA8::CESA8* vector (Fig. 2).

Finally, we examined *ppcesa4/10*KOs and *ppcesa6/7*KOs produced for another study to determine whether they phenocopy the *ppcesa3/8*KO phenotype. Genotype verification for these lines is presented in Fig. S8 and Fig. S9. The *ppcesa4/10*KOs showed slight, but significant reduction in midrib S4B fluorescence. However, for *ppcesa6/7*KOs the reduction was substantial and significant (Fig. 7), showing the PpCESA6/7 and PpCESA3/8 have non-redundant roles in secondary cell wall deposition in leaf midrib cells.

Discussion

PpCESA3 and PpCESA8 function redundantly in cellulose deposition in stereid secondary cell walls.

Targeted knockout of *PpCESA3* and *PpCESA8* blocked deposition of cellulose in the thick walls of stereid cells as indicated by 1) reduction of the strong birefringence associated with the midribs in *ppcesa3/8*KOs, 2) reduction in the midrib fluorescence of *ppcesa3/8*KO leaves stained with S4B, 3) lack of CBM3a labeling of sections from *ppcesa3/8*KO leaf midribs (Fig. 1), and 4) reduction in *ppcesa3/8*KO gametophore cell wall cellulose content as measured by Updegraff assay. Evidence that knockout of *PpCESA3* and *PpCESA8* is responsible for the observed phenotype includes consistency of the phenotype in three independent KOs and restoration of cellulose deposition in the midribs by transformation of *ppcesa3/8*KO with vectors driving expression of PpCESA3 or PpCESA8 (Fig. 2). Whereas we detected no reduction in midrib cellulose in *ppcesa3*KO, the phenotypes of *ppcesa8*KOs were intermediate between wild type and *ppcesa3/8*KO (Fig. 2). This, combined with the observations that only *PpCESA8* is up-regulated to compensate for loss of its paralog (Fig. 6) and expression of PpCESA3 under control of

its native promoter only partially restores the wild type phenotype (Fig. 2), are consistent with the hypothesis that the PpCESA3 and PpCESA8 proteins are functionally interchangeable and that a dosage effect is responsible for the *ppcesa8*KO phenotype. The formation of morphologically normal gametophores in *ppcesa3/8*KOs (Fig. 1) indicates that PpCESA3 and PpCESA8 serve a different role in development than PpCESA5, which supports normal cell division and cell expansion required for gametophore development (Goss et al. 2012). It is possible that PpCESA3 and PpCESA8 contribute to primary cell wall deposition since *ppcesa3/8*KO lamina cells had thinner external walls (Fig. S4) and tended to collapse during embedding (Fig. 1). Alternatively, PpCESA3 and PpCESA8 may contribute to secondary thickening of lamina cell walls after they stop expanding.

CESA evolution in both *P. patens* and Arabidopsis involve sub-functionalization and neo-functionalization.

There are many parallels in the evolution of the *P. patens* and Arabidopsis *CESA* families. In both species, different CESAs are responsible for primary and secondary cell wall deposition. In Arabidopsis, the secondary CESAs are AtCESA4, -7 and -8 (Taylor et al. 2003) and primary CESAs are AtCESA1,-3, and members of the 6-like group (Desprez et al. 2007; Persson et al. 2007). In *P. patens,* midrib secondary cell wall synthesis involves PpCESA3, -6, -7 and -8, whereas gametophore primary cell wall synthesis requires PpCESA5 (Goss et al. 2012). At least some primary CESAs can substitute for secondary CESAs and vice versa in both species. In Arabidopsis, *AtCESA3pro::AtCESA7* partially rescues *atcesa3*, and *AtCESA8pro::AtCESA1* partially rescues *atcesa8* (Carroll et al. 2012). In *P. patens*, *PpCESA8pro::PpCESA5* rescues *ppcesa3/8*KO. This indicates that the *CESA* division of labor for primary and secondary cell wall deposition in vascular plants and mosses is due at least in part to sub-functionalization. However, neo-functionalization has also occurred in both species, resulting in the requirement for two or more non-interchangeable CESA isoforms for secondary cell wall biosynthesis. In Arabidopsis, *atcesa4*, *atcesa7,* and *atcesa8* null mutants share a phenotype (Taylor et al. 2000) that cannot be complemented by expressing one of the other secondary AtCESAs with the promoter for the missing isoform (Kumar et al. 2016). Likewise in *P. patens, ppcesa3/8*KO *and ppcesa6/7*KO share the same phenotype and *ppcesa3/8*KO is not complemented by *PpCESA8pro*::*PpCESA7*. Studies are ongoing to determine whether the secondary PpCESAs physically interact to form a CSC, as has been shown for the secondary AtCESAs (Taylor et al. 2003; Timmers et al. 2009). Finally, the *CESA* families of both species show some redundancy. In Arabidopsis the 6-like *CESA*s (*AtCESA2, -5, -6* and *-9*) are partially redundant (Persson et al. 2007), as are *PpCESA3* and *-8* in *P. patens*. PpCESA6 and -7 differ by only three amino acids and the genes that encode them appear to be redundant (Wise et al. 2011).

A recent study has shown that secondary cell wall deposition, including CESA expression, is regulated by NAC transcription factors in both *P. patens* and Arabidopsis (Xu et al. 2014). Three *P. patens* NAC genes, *PpVNS1*, *PpVNS6*, and *PpVNS7*, were preferentially expressed in leaf midribs and *ppvns1/ppvns6/ppvns7*KOs were defective in stereid development. Overexpression of *PpVNS7* activated PpCESA3 (Xu et al. 2014). Phylogenetic analyses of NACs place eight *PpVNS* proteins within the clade that has variously been named subfamily NAC-c (Shen et al. 2009), subfamily Ic (Zhu et al. 2012), or the VNS group (Xu et al. 2014), and also includes the Arabidopsis vascular-related NACs VND6 (ANAC101), VND7 (ANA030), NST1 (ANAC043), NST2 (ANAC066) and NST3/SND1 (ANAC012). However, the three *PpVNS* genes that regulate stereid development cluster with five other *P. patens* genes implicated in other processes, whereas the angiosperm genes cluster in clades that include members from divergent species (Xu et al. 2014). This is similar to CESA phylogenies, in which *P. patens* proteins are excluded from the clades that comprise each of the six functionally distinct seed plant CESAs (Kumar et al. 2016; Roberts and Bushoven 2007; Yin et al. 2009) and indicates that CESA sub-functionalization occurred independently in mosses and seed plants.

Secondary cell wall microfibrillar texture is similar in mosses and vascular plants.

In vascular plants, both water conducting tracheary elements and supportive fibers are characterized by helical (Barnett and Bonham 2004) and aggregated (Donaldson 2007; Fernandes et al. 2011; Thomas et al. 2014) cellulose microfibrils. The midribs of *P. patens* leaves include hydroid cells that transport water and stereid cells that provide support, but only the stereids have thick cell walls (Xu et al. 2014). With highly reduced cellulose in their stereid secondary cell walls, *ppcesa3/8*KOs provided a negative control for structural characterization of secondary cell walls in wild type *P. patens*. A sharp SFG CH/CH_2 stretch peak at 2944 cm^{-1} is characteristic of angiosperm secondary cell walls (Park et al. 2013) and extensive empirical testing has shown that this spectral feature is attributable to lateral microfibril aggregation (Lee et al. 2014). The 2944 cm^{-1} peak was also present in SFG spectra of wild type *P. patens* midribs. In contrast, the spectra of *ppcesa3/8*KO leaf midribs lacked the 2944 cm^{-1} peak and instead had a broad peak between 2800 and 3000 cm^{-1}, which is characteristic of primary cell walls and other samples lacking aggregated microfibrils (Lee et al. 2014; Park et al. 2013). This suggests that lateral aggregation of microfibrils is a common feature of the secondary cell walls of moss stereids and vascular plant tracheary elements and fibers. Polarization microscopy with a first order retardation plate revealed that the microfibrils in the stereid cell walls are deposited in a helical pattern, as observed in secondary cell walls of tracheary elements and fibers (Barnett and Bonham 2004). Although deficient in cellulose, the stereid cell walls of *ppcesa3/8*KOs were thickened, indicating that secondary cell wall synthesis involves deposition of non-cellulosic components, which proceeded in the absence of cellulose deposition. This

has also been observed in developing tracheary elements treated with cellulose synthesis inhibitors (Taylor et al. 1992). Thus, stereid cell walls share structural characteristics with the cell walls of tracheary elements and fibers.

Mosses and vascular plants have acquired similar secondary cell walls through convergent evolution.

Thick, cellulose-rich secondary cell walls provide added support for aerial organs of mosses and vascular plants alike. Within these cell walls, the lateral aggregation and helical orientation of the microfibrils contributes to their strength and resiliency. Although cortical microtubules play an important role in cellulose microfibril orientation, oriented cellulose deposition can occur in the absence of cortical microtubules, and it has previously been suggested that aggregation and helical orientation of microfibrils in secondary walls is a consequence of high CSC density during rapid cellulose deposition (Emons and Mulder 2000; Lindeboom et al. 2008). Regulation at the level of CSC secretion was emphasized in this model (Emons and Mulder 2000), but CSC density can potentially be regulated at the level of transcription.

Rapid cellulose synthesis during secondary cell wall deposition in specific cell types requires precise temporal and spatial regulation of CESA expression that is distinct from the regulatory requirements for primary cell wall synthesis. We suggest that these distinct regulatory needs were met through the evolution of independent regulatory control of primary and secondary CESAs by sub-functionalization in both mosses and seed plants. In seed plants, phylogenetic analysis shows that the first divergence of the *CESA* family separated the genes that encode the primary and secondary CESAs and was followed by independent diversification within each group (Roberts et al. 2012). This, along with evidence that some primary CESAs are interchangeable with secondary CESAs (Carroll et al. 2012), indicates that sub-functionalization was an early event in the evolution of the seed plant CESA family. In *P. patens*, the genes that encode secondary PpCESA3 and PpCESA8 and primary PpCESA5 are also sub-functionalized and therefore specialized, although they encode interchangeable proteins.

Several lines of evidence indicate that the capacity to deposit a secondary cell wall evolved independently in mosses and seed plants. Structural and paleobotanical evidence suggests that the support and water-conducting cells of bryophytes and vascular plants are not homologous (Carafa et al. 2005; Ligrone et al. 2002). Phylogenetic evidence indicates that the primary and secondary CESAs diversified independently in mosses and seed plants (Kumar et al. 2016; Roberts and Bushoven 2007; Yin et al. 2009) and, as explained above, so did the NAC transcription factors that regulate the secondary CESAs. There are even examples of convergent evolution of secondary cell walls within the angiosperm lineage. Cotton fiber

secondary cell walls are synthesized by the same CESAs that are responsible for secondary cell wall deposition in tracheary elements and fibers (Haigler et al. 2012), whereas the secondary cell walls of epidermal trichomes are synthesized by the primary CESAs (Betancur et al. 2011). These observations are consistent with independent evolutionary origins for secondary cell walls in different land plant lineages and different cell types within angiosperm lineages.

Taken together, these data indicate that *CESA* duplication, followed by adoption of regulatory elements within the secondary *CESA* promoters that enable control by NAC transcription factors, occurred independently in mosses and vascular plants. The resulting uncoupling of the secondary CESAs from the regulatory constraints associated with primary cell wall deposition, along with a mechanistic linkage between CESA expression and microfibril texture as well as selection for strength and resiliency, may have contributed to the capacity of different plants to synthesize cellulose-rich secondary cell walls with similar microfibrillar textures.

Materials and methods

Vector construction

All primer pairs are shown in Table S1, along with annealing temperatures used for PCR. Amplification programs for Taq Polymerase (New England Biolabs, Ipswich, MA, USA) consisted of a 3 min denaturation at 94°C; 35 cycles of 15 s at 94°C, 30 s at the annealing temperature, and 1 min/kbp at 72°C. Amplification programs for Phusion Polymerase (New England Biolabs) consisted of a 30 s denaturation at 98°C; 35 cycles of 7 s at 98°C, 7 s at the annealing temperature, and 30 s/kbp at 72°C.

To construct the CESA8KO vector, a 3’ homologous region was amplified from *P. patens* genomic DNA with primers 174JB and 193JB using Taq DNA polymerase, cut with Sal1 and BspD1, and cloned into the SalI/BstBI site of pBHSNR (gift of Didier Schaefer, University of Neuchâtel). The resulting plasmid was cut with KasI and NsiI to accept the KasI/NsiI fragment of a 5’ homologous region amplified from *P. patens* genomic DNA with primers 203JB and 185JB (Table S1). The CESA8KO vector was cut with EcoRI and NsiI for transformation into wild type *P. patens*. The CESA3KO, CESA4KO, CESA6/7KO, and CESA10KO vectors were constructed using Gateway Multisite Pro cloning (Invitrogen, Grand Island, NY, USA) as described previously (Roberts et al. 2011). Flanking sequences 5’ and 3’ of the coding regions were amplified with appropriate primer pairs (Table S1) using Phusion DNA polymerase (New England Biolabs) and cloned into pDONR 221 P1-P4 and pDONR 221 P3-P2, respectively, using BP Clonase II (Invitrogen). Similarly, an *nph* selection cassette was amplified from pMBL6 (gift of Jesse Machuka, University of Leeds) cloned into pDONR 221 P3r-P4r. All entry clones were sequence-

verified. For vectors conferring hygromycin resistance, entry clones with flanking sequences in pDONR 221 P1-P4 and pDONR 221 P3-P2 were inserted into BHSNRG (Roberts et al. 2011). For vectors conferring G418 resistance, entry clones with flanking sequences in pDONR 221 P1-P4 and pDONR 221 P3-P2 were linked with the entry clone containing the *nph* selection cassette and inserted into pGEM-gate (Vidali et al. 2009) using LR Clonase II Plus (Invitrogen). The vectors in BHSNRG or pGEM-gate were cut with BsrGI for transformation into wild type or mutant *P. patens* lines.

Expression vectors for HA-tagged PpCESAs under control of *PpCESA* promoters were constructed using Gateway Multisite Pro cloning (Invitrogen). The *PpCESA4* (DQ902545), *PpCESA5* (DQ902546), *PpCESA7* (DQ160224) and *PpCESA8* (DQ902549) coding sequences were amplified from cDNA clones pdp21409, pdp24095, pdp38142 and pdp39044 (RIKEN BioResource Center, Tsukuba, Ibaraki JP), respectively, using forward primers containing a single hemagglutinin (HA) tag and appropriate reverse primers (Table S1) and cloned into pDONR 221 P5-P2 using BP Clonase II (Invitrogen). The *PpCESA3* (XP_001753310) and *PpCESA10* (XP_001776974) coding sequences were similarly amplified from expression vectors. pDONR 221 P1-P5r entry clones containing approximately 2 kB of sequence upstream of the *PpCESA3* or *PpCESA8* start codon (Tran and Roberts 2016), were linked to the sequence verified entry clones containing the *HA-PpCESA* coding sequences and inserted into pSi3(TH)GW (Tran and Roberts 2016) using LR Clonase II Plus (Invitrogen). These vectors target the expression cassettes to the intergenic 108 locus, which can be disrupted with no effect on phenotype (Schaefer and Zryd 1997). Rescue vectors were cut with SwaI for transformation into a *P. patens ppcesa3/8*KO line from which the *hph* resistance cassette had been removed (see below).

Culture and transformation of *P. patens*

Wild type *P. patens* lines (haploid) derived from the sequenced Gransden strain (Rensing et al. 2008) by selfing and propagation from a single spore in 2006 (GD06) or 2011 (GD11) were gifts of Pierre-Francois Perroud, Washington University. Wild type and transformed *P. patens* lines were cultured on basal medium supplemented with ammonium tartrate (BCDAT) as described previously (Roberts et al. 2011). Protoplasts were prepared and transformed as described previously (Roberts et al. 2011). Stable transformants were selected with 50 μg mL^{-1} G418 (CESA3KO vector) or 15 μg mL^{-1} hygromycin (CESA8KO and complementation vectors). The *hph* selection cassette was removed from *ppces3*/*ppcesa8*KO by transforming protoplasts with NLS-Cre-Zeo (Vidali et al. 2010) selecting for 7 d on BCDAT plates containing 50 μg mL^{-1} zeocin, replica plating zeocin resistant colonies on BCDAT with and without 15 μg mL^{-1} hygromycin, and recovering hygromycin-sensitive colonies. Protein expression

was tested by western blot analysis as described previously (Scavuzzo-Duggan et al. 2015) in selected lines transformed with HA-PpCESA expression vectors.

Genotype analysis

For PCR screening, DNA was extracted as described previously (Roberts et al. 2011) and 2.5 μL samples were subjected to 35 cycles of amplification (45 s at 94°C, 45 s at the annealing temperature shown in Table S1, 1 min/kbp at 72°C) with PAQ5000 DNA polymerase (Agilent Technologies, http://www.home.agilent.com/) in 25 μL reactions. Primers used to test for target integration, target-gene disruption, and selection cassette excision are listed in Table S1.

Phenotype analysis

Cell wall birefringence of unfixed leaves mounted in water was examined using an Olympus BHS compound microscope with D Plan-Apo UV 10X/0.4, 20X/0.7, and 40X/0.85 objectives, and polarizer and circular-polarizing analyzer, with and without a first order retardation plate (Olympus, Center Valley, PA, USA). Images were captured with a Leica DFC310FX digital camera with Leica Application Suite software, version 4.2.0 (Leica Microsystems Inc., Buffalo Grove, IL, USA) with manual exposure under identical conditions.

For direct fluorescent labeling of cellulose, whole gametophores (3 per line) dissected from colonies grown for four weeks on solid BCDAT medium were dipped in 100% acetone for 5 sec to permeabilize the cuticle, rinsed in phosphate buffered saline (PBS), incubated in PBS containing 0.01 mg/ml S4B (Anderson et al. 2010) for 30 min, and rinsed in PBS. All fully expanded leaves (12-20) were cut from each gametophore and mounted in PBS. Fluorescence images of each leaf, centered on the brightest part of the midrib, were captured using a Zeiss Axio Imager M2 with 43HE DsRed filter set, Plan-Neofluar 20X/0.5 objective, AxioCam MR R3 camera, and Zen Blue software, version 1.1.2.0 (Carl Zeiss Microscopy, Jena, Germany) under identical conditions using manual exposure. The midrib in each image was selected manually (Fig. S10) and average pixel intensity was measured using ImageJ, Fiji version (Schindelin et al. 2012). For comparison of KOs to the wild type, three independent lines of each KO genotype (n=3) and two independent wild type lines (GD06 and GD11, n=2) were sampled in triplicate. For analysis of rescue lines, three independent explants were sampled for each genetic line (n=3).

For affinity cytochemistry of cellulose, gametophores dissected from colonies grown for two weeks on BCDAT medium were fixed and embedded in LR White resin (Polysciences, Inc., Warrington, PA, USA) as described previously (Kulkarni et al. 2012). Sections (1 μm) were mounted and labeled with CBM3a as described previously (Berry et al. 2016). Images were captured with a Zeiss Axio Imager M2 with 38

Green Fluorescent Protein filter set, EC Plan-Neofluar 40X/0.75 objective, AxioCam MR R3 camera, and Zen Blue software, version 1.1.2.0 (Carl Zeiss Microscopy) under identical conditions using manual exposure. Fluorescence and polarization images were not altered after capture. Bright field and differential interference contrast images were captured using automatic exposure and some images used for illustrative purposes were adjusted for uniformity using the color balance and exposure functions in Photoshop, version CS6 (Adobe Systems, San Jose CA, USA).

*ppcesa3*KOs, *ppcesa8*KOs, and *ppcesa3/8*KOs were tested for changes in caulonema gravitropism and rhizoid development as described previously (Roberts et al. 2011). Images were captured using a Leica M165FC stereomicroscope with Leica DFC310FX camera and Leica Application Suite software, version 4.2.0 (Leica Microsystems Inc.). Caulonema length for each colony was measured as the distance from the edge of the colony to tip of the longest caulonema filament using Leica Application Suite software.

Cell wall analysis

Alcohol insoluble residue (AIR) was prepared from gametophores dissected from 8-10 4-week-old explants of *P. patens* wild type (three samples from independent cultures) and *ppcesa3/8*KO (samples from three independent lines) cultured on BCDAT medium. Tissue was ground in liquid nitrogen and extracted three times, 30 min each, with 70% (v/v) ethanol and once with 100% ethanol and the residue was dried under vacuum. The AIR (~1 mg) was weighed to 0.001 mg and mixed with 1 mL of acetic acid:water:nitric acid (8:2:1, v/v) in screw-cap vials and the suspension was heated in a boiling water bath for 30 min (Updegraff 1969). After cooling, the tubes were centrifuged at 16,900 x g for 5 min and the supernatant discarded. The pellet was resuspended in 2 mL of deionized water, centrifuged, and the supernatant was discarded. The washing step was repeated at least 10 more times until the supernatant was neutralized and the pellet was resuspended in 1 mL of water. The amount of cellulose remaining after hydrolysis was quantified by sulfuric acid assay (Albalasmeh et al. 2013) with glucose as the standard. Briefly, 100 µL of hydrolysate (six technical replicates per sample) was diluted to 1 mL with water in a glass tube, 3 mL of concentrated sulfuric acid was added, and samples were vortexed for 30 s and chilled on ice for 2 min. Reactions were measured at 315 nm against a reagent blank.

High pressure freezing-freeze substitution and transmission electron microscopy

Gametophytes of *P. patens* GD06 and PpCESAKOs were high pressure-frozen using a Leica EMPACT2 high pressure freezer (Leica Microsystems, Inc.) followed by freeze-substitution in 0.1% uranyl acetate in acetone for 48 h at -90^{o}C before the temperature was ramped up slowly to -50^{o}C (Wilson and Bacic 2012). The samples were rinsed with acetone twice at -50^{o}C before the acetone was replaced with ethanol

and the samples were subsequently infiltrated with LR White resin (ProSciTech Pty. Ltd., Thuringowa Central QLD Australia) in a series of ethanol/resin dilutions. The samples were rinsed three times in 100% resin before polymerization with UV light at -20^{o}C for 48 h. Thin sections (70 nm) were cut using a Leica Ultracut R (Leica Microsystems, Inc.) and post-stained with uranyl acetate and lead citrate (Wilson and Bacic 2012). Images were taken using a Tecnai G2 Spirit transmission electron microscope (FEI, Hillsboro, OR USA). Cell wall thickness was measured using ImageJ, Fiji version (Schindelin et al. 2012).

Ultrathin sections (70 nm) were also cut from blocks prepared for affinity cytochemistry (see above), mounted on Formvar coated copper grids, and stained with uranyl acetate and lead citrate (Wilson and Bacic 2012). Sections were imaged using a FEI/Phillips CM-200 transmission electron microscope (FEI).

Sum Frequency Generation spectroscopy

Leaves of wild type GD06, 8KO-5B, and 3/8KO-86 lines were mounted abaxial side down in water on glass slides and allowed to air-dry overnight. SFG spectra were collected 5 µm intervals along a 200 µm line scan perpendicular to the midrib at its thickest point using an SFG microscope system described previously (Lee et al. 2016). The SFG spectra were collected with the following polarization combination: SFG signal = s-, 800 nm = s-, and broadband mid-IR = p-polarized with the laser incidence plane and the laser incidence plane aligned along the axis of midrib.

Reverse transcription quantitative PCR

RNA was extracted from gametophores from two independent wild type and three independent lines each of *pp*cesa3KO and *pp*cesa8KO as described previously (Tran and Roberts 2016). cDNA samples were tested in duplicate as described previously using primer pairs for amplification of *PpCESA3* and PpCESA8. The primers have been previously tested for specificity and efficiency (Tran and Roberts 2016). Primers for actin and v-Type H^{+}translocating pyrophosphatase reference genes were described previously (Le Bail et al. 2013). Target/average reference cross point ratios were calculated for each sample and standard errors were calculated for independent genetic lines.

Statistical analysis

For statistical analysis, one-way Analysis of Variance (ANOVA) with post-hoc Tukey Honest Significant Difference (HSD) test was performed at astatsa.com/OneWay_Anova_with_TukeyHSD/.

Supplemental Materials

Table S1. Primers used for vector construction and genotype analysis.

Fig. S1. Genotype analysis of *ppcesa8*, *ppcesa3* and *ppcesa3/8* KO lines.

Fig. S2: Phenotype analysis of a *ppcesa3/*8 double KO line transformed with vectors driving expression of *PpCESA3* or *PpCESA8* with their native promoters.

Fig. S3. Transmission electron microscopy images of leaf cell walls from wild type and *cesa*KO lines of *P. patens.*

Fig. S4. Thickness of outer cell walls measured from transmission electron microscopy images.

Fig. S5: *P. patens* wild type and KO lines cultured on medium containing 1 μM naphthalene acetic acid (auxin) to induce rhizoid initiation and inhibit leaf initiation.

Fig. S6: *P. patens* wild type and KO lines cultured in the dark on vertically oriented plates containing medium supplemented with 35 mM sucrose to test for caulonema gravitropism.

Fig. S7. Western blot analysis of protein expression for *P. patens* lines derived from transformation of *ppcesa3/8*KO-86lox with vectors driving expression of PpCESAs under control of the *PpCESA8* promoter.

Acknowledgements

This work was supported primarily by National Science Foundation Award IOS-1257047. Analysis of mutants by SFG spectroscopy was supported as part of The Center for LignoCellulose Structure and Formation, an Energy Frontier Research Center funded by the U.S. Department of Energy, Office of Science, Office of Basic Energy Sciences under Award Number DE-SC0001090. CBM3a affinity cytochemistry and freeze substitution transmission electron microscopy were supported by the Australian Research Council Centre for Excellence in Plant Cell Walls Grant CE1101007. High-pressure freezing and transmission electron microscopy was conducted at the Melbourne Advanced Microscopy Facility at the Bio21 Institute and the Biosciences Microscopy Unit at The University of Melbourne. DNA sequencing and qPCR were conducted using the Rhode Island Genomics and Sequencing Center, a Rhode Island NSF EPSCoR research facility, supported in part by the National Science Foundation EPSCoR Cooperative Agreement EPS-1004057. Clones pdp39044 and pdp10281 were from RIKEN BRC. We also thank Chessa Goss and Virginia Lai for preliminary work on *ppceas8*KO, Alfred Schupp for

assistance with vector construction, Evan Preisser for assistance with statistics, and Sarah Kiemle for conducting Updegraff assays.

Tables

Table 1. Caulonema length for wild type and *ppcesa3/8*KOs grown on vertical plates in the dark. Data are from two independent experiments (n=2). ANOVA analysis showed no significant differences between genetic lines.

Genetic line	Caulonema length (mm)	Standard Error
WT GD06	4.69	0.50
*ppcesaA3/8*KO-43	5.70	0.87
*ppcesaA3/8*KO-57	4.51	1.14
*ppcesaA3/8*KO-86	5.69	0.47

Figure legends

Figure 1: Phenotypes of *ppcesa3/8*KO, *ppcesa3*KO and *ppcesa8*KO compared to wild type *Physcomitrella patens*. (A-D) Colony morphology is similar in wild type, *ppcesa*3KOs and *ppcesa*8KOs; horizontal growth is typical of gametophores produced by *ppcesa*3/8KO (arrowheads). (E-H) Polarized light microscopy of leaves shows that the midribs of wild type and *ppcesa*3KO are highly birefringent. The midribs of *ppcesa*3/8KO leaves have low birefringence and *ppcesa*8KO leaves have moderate birefringence. (I-L) Fluorescence microscopy of leaves stained with S4B shows strong fluorescence in the midribs of wild type and *ppcesa*3KO, low fluorescence in the midribs of *ppcesa*3/8KO leaves and intermediate fluorescence in the midribs of *ppcesa*8KO leaves. (M-P) Differential interference contrast microscopy of sections through the midribs of maturing leaves (L=lamina cell, *=bundle sheath cell). In wild type and *ppcesa*3KO, the walls of bundle sheath cells and the stereid cells they surround show enhanced contrast due to higher refractive index. (Q-T) Fluorescence microscopy of the same sections shown in M-P labeled with CBM3a. The bundle sheath and stereid cells of wild type and *ppcesa*3KO leaves are strongly labeled, whereas labeling is weak in *ppcesa*3/8KO and intermediate in *ppcesa*8KO leaves.

Figure 2: Quantitative analysis of S4B fluorescence intensity in leaf midribs of *P. patens* wild type, *ppcesa*KO, and rescue lines. (A) Fluorescence was significantly weaker in *ppcesa*3/8KOs compared to wild type (WT). *ppcesa*3KOs were not significantly different from wild type, whereas *ppcesa8*KOs were intermediate between the wild type and *ppcesa*3/8KOs and significantly different from both. For each mutant genotype, three independent genetic lines were sampled in triplicate. Two independent wild type lines (GD06 and GD11) were sampled in triplicate. Bars indicate the standard error of the mean for three mutant (n=3) or two wild type (n=2) lines. Genotypes with different letters are significantly different. (B) Lines derived from transformation of *ppcesa*3/8KO-86lox with *proCESA8::CESA8* (8R) had significantly higher fluorescence compared to the parent double KO line and *ppcesa*8KO, but significantly less than WT. (C) Lines derived from transformation of *ppcesa*3/8-86lox with *proCESA3::CESA3* (3R) had significantly higher fluorescence compared to the parent double KO line (except 3R29) and were not significantly different from either *ppcesa*8KO lines (3R29 and 3R52) or WT (3R45). For B and C, three independent explants were sampled for each genetic line. Bars indicate the standard error of the mean for three explants from the same line (n=3 or n=2 (WT, 3/8KO, 8KO in C)).

Figure 3: Polarized light microscopy with first order retardation plate. Double pointed arrow indicates the vibration direction of the major axis. (A-C) Midrib of a mature wild type leaf oriented parallel, perpendicular, and at 45^{o} to the major axis of the retardation plate. Bundle sheath cells (*) flank the

central midrib. (D) Midrib of a developing wild type leaf oriented parallel to the major axis of the retardation plate showing change in microfibril orientations through the basal (b), medial (m), and apical (a) regions of the midrib. (E-G) Midrib of a mature *ppcesa*3/8KO leaf oriented parallel, perpendicular, and at 45^{o} to the major axis of the retardation plate. (H) Midrib of a developing *ppcesa*3/8KO leaf oriented parallel to the major axis of the retardation plate showing no change in microfibril orientation through the basal, medial, and apical regions of the leaf. Bar in A is also for B-C and E-G and bar in D is also for H.

Figure 4: Transmission electron microscopy images of leaf midribs of *P. patens* showing adjacent cells with primary cell walls (PW) and secondary cell walls (SW) in (A) wild type, and (B-D) mutant leaves.

Figure 5: Sum Frequency Generation (SFG) spectroscopy of *P. patens* leaves. (A) Full SFG spectra collected from leaf midribs (each is the average of nine spectra, from three different positions on each of three different leaves). A strong peak in the C-H stretch region (2944 cm^{-1}) is present in spectra from wild type (WT), greatly diminished in spectra from *ppcesa8*KO (8KO), and absent in spectra from *ppcesa3/8*KO (3/8KO). (B) *P. patens* wild type, *ppcesa8*KO, and *ppcesa3/8*KO leaves with SFG scan trajectories traversing the midribs. Step size was 5 μm/step. SFG spectra were collected from 2850 to 3150 cm^{-1}, covering the entire CH region. (C) 2D projection image of SFG spectra collected across the midribs of each leaf shown in B. Each column in each image is an entire spectrum collected from one point plotted against displacement along the scan trajectory. Colors indicate SFG intensity as shown in the legend.

Figure 6: RT-qPCR analysis of *PpCESA3* and *PpCESA8* expression in wild type, *ppcesa3*KOs and *ppcesa8*KOs. Target/average reference cross point ratios (using actin and v-Type H^{+}translocating pyrophosphatase reference genes) were determined for three independent lines of each mutant (3KO-5, -35, -126; 8KO-5B, -4C, -10C; and 3/8KO-43, -57, -86) and two independent wild type lines (GD06 and GD11) with two technical replicates each. Bars indicate the standard error of the mean for the three mutant (n=3) or two wild type (n=2) lines.

Figure 7: Quantitative analysis of S4B fluorescence intensity in leaf midribs. (A,B) Wild type (WT), *ppcesa*3/8KO-86lox, and *ppcesa*3/8KO-86lox transformed with *proCESA8::CESA* expression vectors. For each rescue genotype, three independent genetic lines were sampled in triplicate and measured with 6 samples of wild type (GD06) and 8 samples of *ppcesa*3/8KO-86lox. (A) For lines derived from transformation of *ppcesa*3/8KO-86lox with *proCESA8::CESA3* (8pro:3R), *proCESA8::CESA7* (pro8:7R), and *proCESA8::CESA10* (pro8:10R) genotypes, the three independent lines did not differ significantly and were combined. *proCESA8::CESA7* and *proCESA8::CESA10* lines did not differ significantly from

the parent double KO line ($p > 0.05$), whereas *proCESA8::CESA3* lines had significantly higher fluorescence compared to the parent double KO line, but significantly less than WT ($p < 0.05$). Bars indicate the standard error of the mean for three independent lines. Genotypes with different letters are significantly different. (B) For lines derived from transformation of *ppcesa*3/8KO-86lox with *proCESA8::CESA5* (pro8:5R) and *proCESA8::CESA4* (pro8:4R), the three independent lines were significantly different and were analyzed separately. *proCESA8::CESA5* (5R) lines were not significantly different from the wild type ($p > 0.05$), except for 5R7, which was not significantly different from *ppcesa*3/8KO-86lox ($p > 0.05$). *proCESA8::CESA5* lines did not differ significantly from *ppcesa*3/8KO-86lox ($p > 0.05$). Bars indicate the standard error of the mean for three gametophores from the same line (n=3). Lines with different letters are significantly different ($p < 0.05$. (C) Mid rib fluorescence was slightly, but significantly reduced in *cesa4/10*KO compared to wild type ($p = 0.037$). Reduction in midrib fluorescence in *cesa6/7*KO was substantial and highly significant ($p = 0.0011$). Bars indicate the standard error of the mean for three independent mutant lines or 3 replicates of wild type (n=3).

References cited:

Albalasmeh AA, Berhe AA, Ghezzehei TA (2013) A new method for rapid determination of carbohydrate and total carbon concentrations using UV spectrophotometry. Carbohydr Polym 97: 253-261

Anderson CT, Carroll A, Akhmetova L, Somerville C (2010) Real-time imaging of cellulose reorientation during cell wall expansion in Arabidopsis roots. Plant Physiol 152: 787-796

Barnett JR, Bonham VA (2004) Cellulose microfibril angle in the cell wall of wood fibres. Biol Rev Camb Philos Soc 79: 461-472

Barnette AL, Bradley LC, Veres BD, Schreiner EP, Park YB, Park J, Park S, Kim SH (2011) Selective detection of crystalline cellulose in plant cell walls with sum-frequency-generation (SFG) vibration spectroscopy. Biomacromolecules 12: 2434-2439

Barnette AL, Lee C, Bradley LC, Schreiner EP, Park YB, Shin H, Cosgrove DJ, Park S, Kim SH (2012) Quantification of crystalline cellulose in lignocellulosic biomass using sum frequency generation (SFG) vibration spectroscopy and comparison with other analytical methods. Carbohydr Polym 89: 802-809

Berry EA, Tran ML, Dimos CS, Budziszek MJ, Jr., Scavuzzo-Duggan TR, Roberts AW (2016) Immuno and affinity cytochemical analysis of cell wall composition in the moss *Physcomitrella patens*. Front Plant Sci 7: 248

Betancur L, Singh B, Rapp RA, Wendel JF, Marks MD, Roberts AW, Haigler CH (2011) Phylogenetically distinct cellulose synthase genes support secondary wall thickening in arabidopsis shoot trichomes and cotton fiber. J Integr Plant Biol 52: 205-220

Blake AW, McCartney L, Flint JE, Bolam DN, Boraston AB, Gilbert HJ, Knox JP (2006) Understanding the biological rationale for the diversity of cellulose-directed carbohydrate-binding modules in prokaryotic enzymes. J Biol Chem 281: 29321-29329

Carafa A, Duckett JG, Knox JP, Ligrone R (2005) Distribution of cell-wall xylans in bryophytes and tracheophytes: new insights into basal interrelationships of land plants. New Phytol 168: 231-240

Carpita N, McCann M (2000) The cell wall. In: Buchanan B, Gruissem W, Jones R (eds) Biochemistry and Molecular Biology of Plants. American Society of Plant Physiologists, Rockville, MD, pp 52-108

Carroll A, Mansoori N, Li S, Lei L, Vernhettes S, Visser RG, Somerville C, Gu Y, Trindade LM (2012) Complexes with mixed primary and secondary cellulose synthases are functional in Arabidopsis plants. Plant Physiol 160: 726-737

Delmer DP (1999) Cellulose biosynthesis: Exciting times for a difficult field of study. Annu Rev Plant Physiol Plant Mol Biol 50: 245-276

Desprez T, Juraniec M, Crowell EF, Jouy H, Pochylova Z, Parcy F, Hofte H, Gonneau M, Vernhettes S (2007) Organization of cellulose synthase complexes involved in primary cell wall synthesis in Arabidopsis thaliana. Proc. Natl. Acad. Sci. USA 104: 15572-15577

Donaldson L (2007) Cellulose microfibril aggregates and their size variation with cell wall type. Wood Sci Technol 41: 443-460

Emons AMC, Mulder BM (2000) How the deposition of cellulose microfibrils builds cell wall architecture. Trends Plant Sci 35-40

Fernandes AN, Thomas LH, Altaner CM, Callow P, Forsyth VT, Apperley DC, Kennedy CJ, Jarvis MC (2011) Nanostructure of cellulose microfibrils in spruce wood. Proc Natl Acad Sci U S A 108: E1195-1203

Gonneau M, Desprez T, Guillot A, Vernhettes S, Hofte H (2014) Catalytic subunit stoichiometry within the cellulose synthase complex. Plant Physiol 166: 1709-1712

Goss CA, Brockmann DJ, Bushoven JT, Roberts AW (2012) A *CELLULOSE SYNTHASE* (*CESA*) gene essential for gametophore morphogenesis in the moss *Physcomitrella patens*. Planta 235: 1355-1367

Haigler CH, Betancur L, Stiff MR, Tuttle JR (2012) Cotton fiber: a powerful single-cell model for cell wall and cellulose research. Front Plant Sci 3: 104

Hebant C (1977) The Conducting Tissues of Bryophytes. J. Cramer, Vaduz

Hill JL, Jr., Hammudi MB, Tien M (2014) The Arabidopsis cellulose synthase complex: a proposed hexamer of CESA trimers in an equimolar stoichiometry. Plant Cell 26: 4834-4842

Jarvis MC (2013) Cellulose biosynthesis: counting the chains. Plant Physiol 163: 1485-1486

Kenrick P, Crane PR (1997) The origin and early evolution of plants on land. Nature 389: 33-39

Kimura S, Laosinchai W, Itoh T, Cui X, Linder CR, Brown RM, Jr. (1999) Immunogold labeling of rosette terminal cellulose-synthesizing complexes in the vascular plant *Vigna angularis*. Plant Cell 11: 2075-2085

Kulkarni AR, Peña MJ, Avci U, Mazumder K, Urbanowicz BR, Pattathil S, Yin Y, O'Neill MA, Roberts AW, Hahn MG, Xu Y, Darvill AG, York WS (2012) The ability of land plants to synthesize glucuronoxylans predates the evolution of tracheophytes. Glycobiology 22: 439–451

Kumar M, Atanassov I, Turner S (2016) Functional analysis of cellulose synthase CESA protein class-specificity. Plant Physiol 173: 970-983

Le Bail A, Scholz S, Kost B (2013) Evaluation of reference genes for RT qPCR analyses of structure-specific and hormone regulated gene expression in *Physcomitrella patens* gametophytes. PLoS One 8: e70998

Lee CM, Kafle K, Huang S, Kim SH (2016) Multimodal Broadband Vibrational Sum Frequency Generation (MM-BB-V-SFG) Spectrometer and Microscope. J Phys Chem B 120: 102-116

Lee CM, Kafle K, Park YB, Kim SH (2014) Probing crystal structure and mesoscale assembly of cellulose microfibrils in plant cell walls, tunicate tests, and bacterial films using vibrational sum frequency generation (SFG) spectroscopy. Phys Chem Chem Phys 16: 10844-10853

Ligrone R, Vaughn KC, Renzaglia KS, Knox JP, Duckett JG (2002) Diversity in the distribution of polysaccharide and glycoprotein epitopes in the cell walls of bryophytes: new evidence for the multiple evolution of water-conducting cells. New Phytol 156: 491-508

Lindeboom J, Mulder BM, Vos JW, Ketelaar T, Emons AM (2008) Cellulose microfibril deposition: coordinated activity at the plant plasma membrane. J Microsc 231: 192-200

Newman RH, Hill SJ, Harris PJ (2013) Wide-angle x-ray scattering and solid-state nuclear magnetic resonance data combined to test models for cellulose microfibrils in mung bean cell walls. Plant Physiol 163: 1558-1567

Nixon BT, Mansouri K, Singh A, Du J, Davis JK, Lee JG, Slabaugh E, Vandavasi VG, O'Neill H, Roberts EM, Roberts AW, Yingling YG, Haigler CH (2016) Comparative structural and computational analysis supports eighteen cellulose synthases in the plant cellulose synthesis complex. Sci Rep 6: 28696

Oehme DP, Downton MT, Doblin MS, Wagner J, Gidley MJ, Bacic A (2015) Unique aspects of the structure and dynamics of elementary Ibeta cellulose microfibrils revealed by computational simulations. Plant Physiol 168: 3-17

713 Park YB, Lee CM, Koo BW, Park S, Cosgrove DJ, Kim SH (2013) Monitoring meso-scale ordering of
714 cellulose in intact plant cell walls using sum frequency generation spectroscopy. Plant Physiol
715 163: 907-913
716 Persson S, Paredez A, Carroll A, Palsdottir H, Doblin M, Poindexter P, Khitrov N, Auer M, Somerville
717 CR (2007) Genetic evidence for three unique components in primary cell-wall cellulose synthase
718 complexes in Arabidopsis. Proc. Natl. Acad. Sci. USA 104: 15566-15571
719 Rensing SA, Lang D, Zimmer AD, Terry A, Salamov A, Shapiro H, Nishiyama T, Perroud PF, Lindquist
720 EA, Kamisugi Y, Tanahashi T, Sakakibara K, Fujita T, Oishi K, Shin IT, Kuroki Y, Toyoda A,
721 Suzuki Y, Hashimoto S, Yamaguchi K, Sugano S, Kohara Y, Fujiyama A, Anterola A, Aoki S,
722 Ashton N, Barbazuk WB, Barker E, Bennetzen JL, Blankenship R, Cho SH, Dutcher SK, Estelle
723 M, Fawcett JA, Gundlach H, Hanada K, Heyl A, Hicks KA, Hughes J, Lohr M, Mayer K,
724 Melkozernov A, Murata T, Nelson DR, Pils B, Prigge M, Reiss B, Renner T, Rombauts S,
725 Rushton PJ, Sanderfoot A, Schween G, Shiu SH, Stueber K, Theodoulou FL, Tu H, Van de Peer
726 Y, Verrier PJ, Waters E, Wood A, Yang L, Cove D, Cuming AC, Hasebe M, Lucas S, Mishler
727 BD, Reski R, Grigoriev IV, Quatrano RS, Boore JL (2008) The *Physcomitrella* genome reveals
728 evolutionary insights into the conquest of land by plants. Science 319: 64-69
729 Roberts AW, Bushoven JT (2007) The cellulose synthase (*CESA*) gene superfamily of the moss
730 *Physcomitrella patens*. Plant Mol Biol 63: 207-219
731 Roberts AW, Dimos C, Budziszek MJ, Goss CA, Lai V (2011) Knocking out the wall: protocols for gene
732 targeting in *Physcomitrella patens*. Methods Mol Biol 715: 273-290
733 Roberts AW, Roberts EM, Haigler CH (2012) Moss cell walls: structure and biosynthesis. Front Plant Sci
734 3: 166
735 Scavuzzo-Duggan TR, Chaves AM, Roberts AW (2015) A complementation assay for in vivo protein
736 structure/function analysis in *Physcomitrella patens* (Funariaceae). App Plant Sci 3: 1500023
737 Schaefer DG, Zryd JP (1997) Efficient gene targeting in the moss *Physcomitrella patens*. Plant J 11:
738 1195-1206
739 Schindelin J, Arganda-Carreras I, Frise E, Kaynig V, Longair M, Pietzsch T, Preibisch S, Rueden C,
740 Saalfeld S, Schmid B, Tinevez JY, White DJ, Hartenstein V, Eliceiri K, Tomancak P, Cardona A
741 (2012) Fiji: an open-source platform for biological-image analysis. Nat Methods 9: 676-682
742 Schuetz M, Smith R, Ellis B (2013) Xylem tissue specification, patterning, and differentiation
743 mechanisms. J Exp Bot 64: 11-31
744 Shen H, Yin Y, Chen F, Xu Y, Dixon RA (2009) A bioinformatic analysis of NAC genes for plant cell
745 wall development in relation to lignocellulosic bioenergy production. Bioenerg Res 2: 217-232

746 Taylor JG, Owen TP, Jr., Koonce LT, Haigler CH (1992) Dispersed lignin in tracheary elements treated
747 with cellulose synthesis inhibitors provides evidence that molecules of the secondary cell wall
748 mediate wall patterning. Plant J 2: 959-970
749 Taylor NG, Gardiner JC, Whiteman R, Turner SR (2004) Cellulose synthesis in the Arabidopsis
750 secondary cell wall. Cellulose 11: 329-338
751 Taylor NG, Howells RM, Huttly AK, Vickers K, Turner SR (2003) Interactions among three distinct
752 CesA proteins essential for cellulose synthesis. Proc Natl Acad Sci USA 100: 1450-1455
753 Taylor NG, Laurie S, Turner SR (2000) Multiple cellulose synthase catalytic subunits are required for
754 cellulose synthesis in Arabidopsis. Plant Cell 12: 2529-2539
755 Thomas LH, Forsyth VT, Martel A, Grillo I, Altaner CM, Jarvis MC (2014) Structure and spacing of
756 cellulose microfibrils in woody cell walls of dicots. Cellulose 21: 3887-3895
757 Timmers J, Vernhettes S, Desprez T, Vincken JP, Visser RG, Trindade LM (2009) Interactions between
758 membrane-bound cellulose synthases involved in the synthesis of the secondary cell wall. FEBS
759 Lett. 583: 978-982
760 Tran ML, Roberts AW (2016) *Cellulose synthase* (*CESA*) gene expression profiling of *Physcomitrella*
761 *patens*. . Plant Biol 18: 362–368
762 Updegraff DM (1969) Semimicro determination of cellulose in biological materials. Anal Biochem 32:
763 420-424
764 Vandavasi VG, Putnam DK, Zhang Q, Petridis L, Heller WT, Nixon BT, Haigler CH, Kalluri U, Coates
765 L, Langan P, Smith JC, Meiler J, O'Neill H (2016) A structural study of CESA1 catalytic domain
766 of Arabidopsis cellulose synthesis complex: evidence for CESA trimers. Plant Physiol 170: 123-
767 135
768 Vidali L, Burkart GM, Augustine RC, Kerdavid E, Tuzel E, Bezanilla M (2010) Myosin XI is essential
769 for tip growth in Physcomitrella patens. Plant Cell 22: 1868-1882
770 Vidali L, van Gisbergen PA, Guerin C, Franco P, Li M, Burkart GM, Augustine RC, Blanchoin L,
771 Bezanilla M (2009) Rapid formin-mediated actin-filament elongation is essential for polarized
772 plant cell growth. Proc Natl Acad Sci U S A 106: 13341-13346
773 Wilson SM, Bacic A (2012) Preparation of plant cells for transmission electron microscopy to optimize
774 immunogold labeling of carbohydrate and protein epitopes. Nat Protoc 7: 1716-1727
775 Wise HZ, Saxena IM, Brown RM, Jr. (2011) Isolation and characterization of the cellulose synthase
776 genes *PpCesA6* and *PpCesA7* in *Physcomitrella patens*. Cellulose 18: 371-384
777 Xu B, Ohtani M, Yamaguchi M, Toyooka K, Wakazaki M, Sato M, Kubo M, Nakano Y, Sano R,
778 Hiwatashi Y, Murata T, Kurata T, Yoneda A, Kato K, Hasebe M, Demura T (2014) Contribution
779 of NAC transcription factors to plant adaptation to land. Science 343: 1505-1508

780 Yang JH, Wang H (2016) Molecular mechanisms for vascular development and secondary cell wall
781 formation. Front Plant Sci 7: 356
782 Yin Y, Huang J, Xu Y (2009) The cellulose synthase superfamily in fully sequenced plants and algae.
783 BMC Plant Biol 9: 99
784 Zhong R, Ye ZH (2015) Secondary cell walls: biosynthesis, patterned deposition and transcriptional
785 regulation. Plant Cell Physiol 56: 195-214
786 Zhu T, Nevo E, Sun D, Peng J (2012) Phylogenetic analyses unravel the evolutionary history of NAC
787 proteins in plants. Evolution 66: 1833-1848

788

789

790

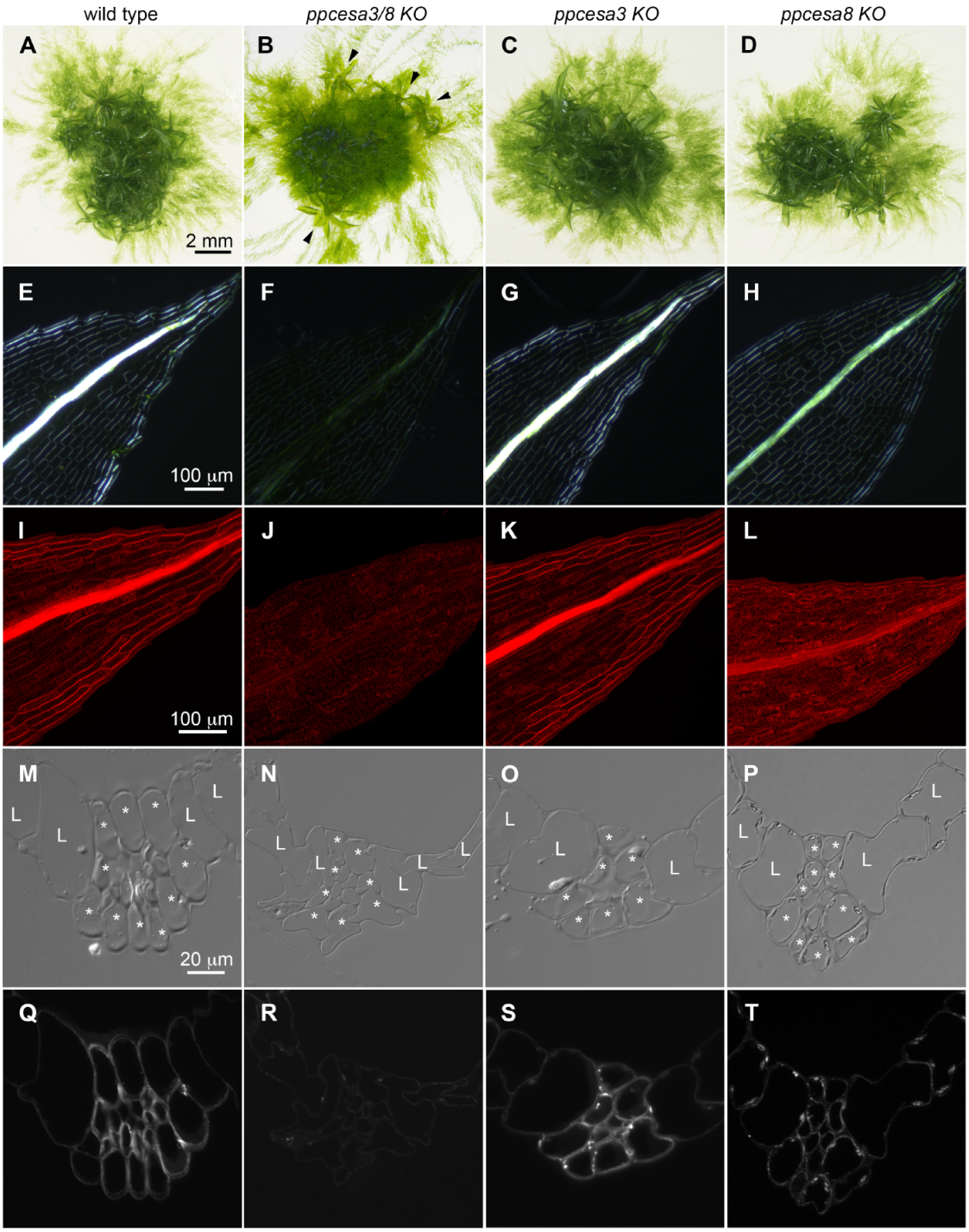

Figure 1: Phenotypes of *ppcesa3/8*KO, *ppcesa3*KO and *ppcesa8*KO compared to wild type *Physcomitrella patens*. (A-D) Colony morphology is similar in wild type, *ppcesa*3KOs and *ppcesa*8KOs; horizontal growth is typical of gametophores produced by *ppcesa*3/8KO (arrowheads). (E-H) Polarized light microscopy of leaves shows that the midribs of wild type and *ppcesa*3KO are highly birefringent. The midribs of *ppcesa*3/8KO leaves have low birefringence and *ppcesa*8KO leaves have moderate birefringence. (I-L) Fluorescence microscopy of leaves stained with S4B shows strong fluorescence in the midribs of wild type and *ppcesa*3KO, low fluorescence in the midribs of *ppcesa*3/8KO leaves and intermediate fluorescence in the midribs of *ppcesa*8KO leaves. (M-P) Differential interference contrast microscopy of sections through the midribs of maturing leaves (L=lamina cell, *=bundle sheath cell). In wild type and *ppcesa*3KO, the walls of bundle sheath cells and the stereid cells they surround show enhanced contrast due to higher refractive index. (Q-T) Fluorescence microscopy of the same sections shown in M-P labeled with CBM3a. The bundle sheath and stereid cells of wild type and *ppcesa*3KO leaves are strongly labeled, whereas labeling is weak in *ppcesa3/8*KO and intermediate in *ppcesa*8KO leaves.

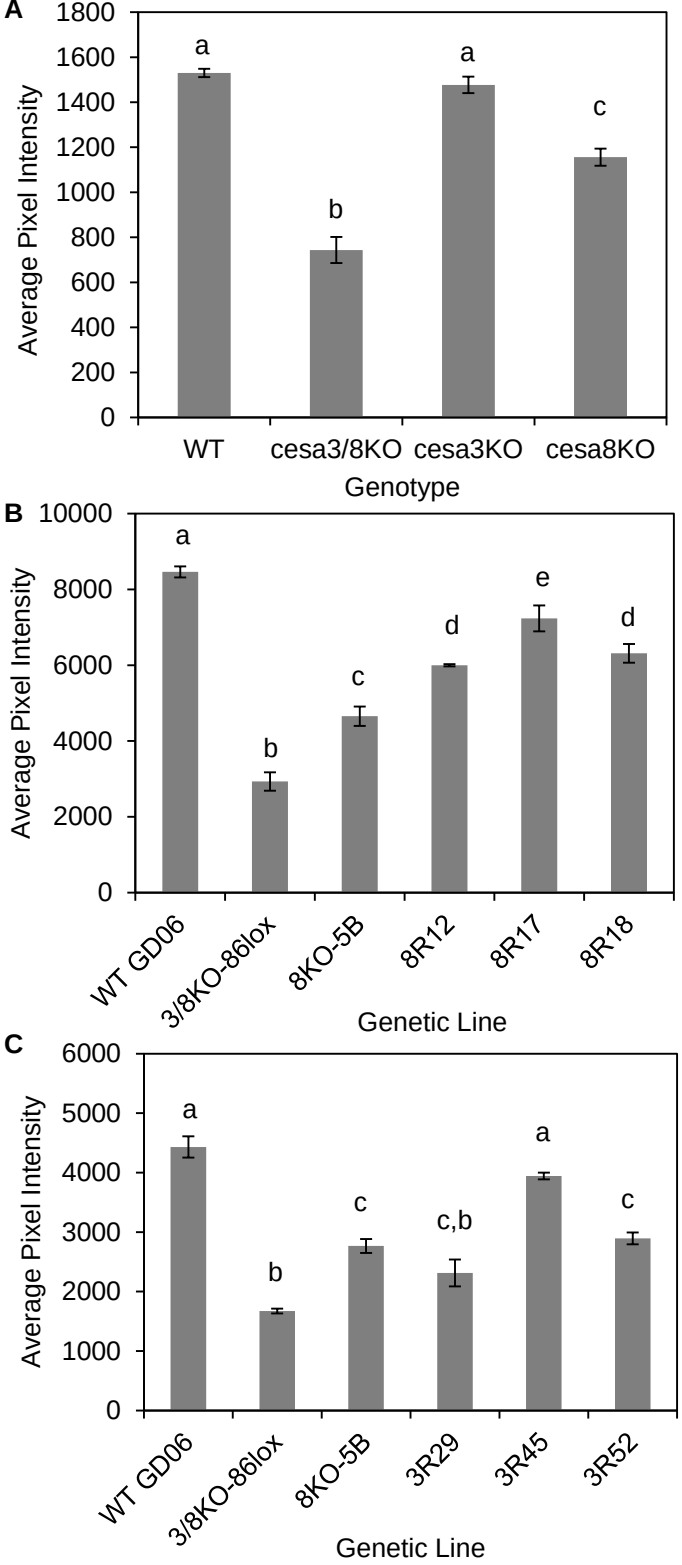

Figure 2: Quantitative analysis of S4B fluorescence intensity in leaf midribs of *P. patens* wild type, *ppcesa*KO, and rescue lines. (A) Fluorescence was significantly weaker in *ppcesa*3/8KOs compared to wild type (WT). *ppcesa*3KOs were not significantly different from wild type, whereas *ppcesa8*KOs were intermediate between the wild type and *ppcesa*3/8KOs and significantly different from both. For each mutant genotype, three independent genetic lines were sampled in triplicate. Two independent wild type lines (GD06 and GD11) were sampled in triplicate. Bars indicate the standard error of the mean for three mutant (n=3) or two wild type (n=2) lines. Genotypes with different letters are significantly different. (B) Lines derived from transformation of *ppcesa*3/8KO-86lox with *proCESA8::CESA8* (8R) had significantly higher fluorescence compared to the parent double KO line and *ppcesa*8KO, but significantly less than WT. (C) Lines derived from transformation of *ppcesa*3/8-86lox with *proCESA3::CESA3* (3R) had significantly higher fluorescence compared to the parent double KO line (except 3R29) and were not significantly different from either *ppcesa*8KO lines (3R29 and 3R52) or WT (3R45). For B and C, three independent explants were sampled for each genetic line. Bars indicate the standard error of the mean for three explants from the same line (n=3 or n=2 (WT, 3/8KO, 8KO in C)).

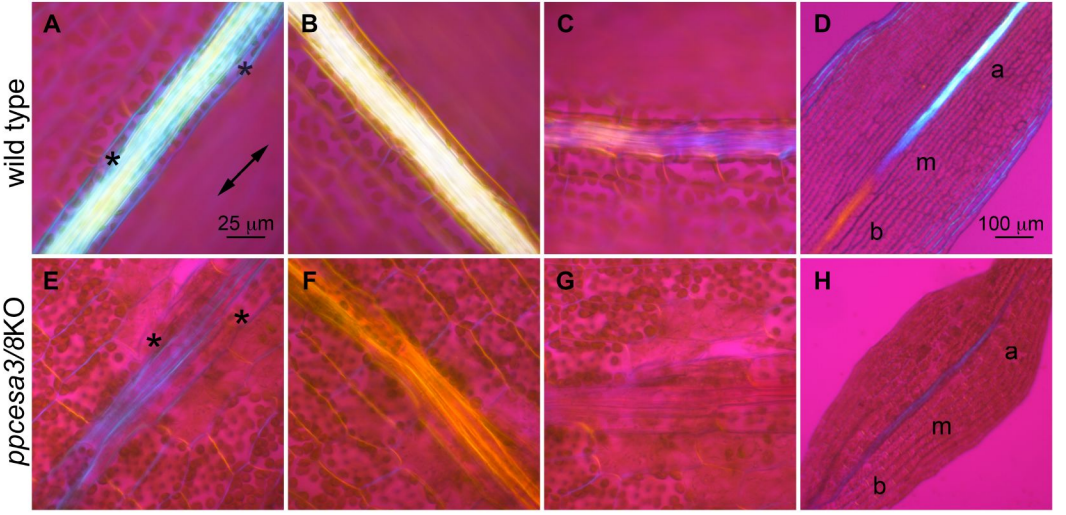

Figure 3: Polarized light microscopy with red I retardation plate. Double pointed arrow indicates the vibration direction of the major axis. (A-C) Midrib of a mature wild type leaf oriented parallel, perpendicular, and at 45° to the major axis of the retardation plate. Bundle sheath cells (*) flank the central midrib. (D) Midrib of a developing wild type leaf oriented parallel to the major axis of the retardation plate showing change in microfibril orientations through the basal (b), medial (m), and apical (a) regions of the midrib. (E-G) Midrib of a mature *ppcesa*3/8KO leaf oriented parallel, perpendicular, and at 45° to the major axis of the retardation plate. (H) Midrib of a developing *ppcesa*3/8KO leaf oriented parallel to the major axis of the retardation plate showing no change in microfibril orientation through the basal, medial, and apical regions of the leaf. Bar in A is also for B-C and E-G and bar in D is also for H.

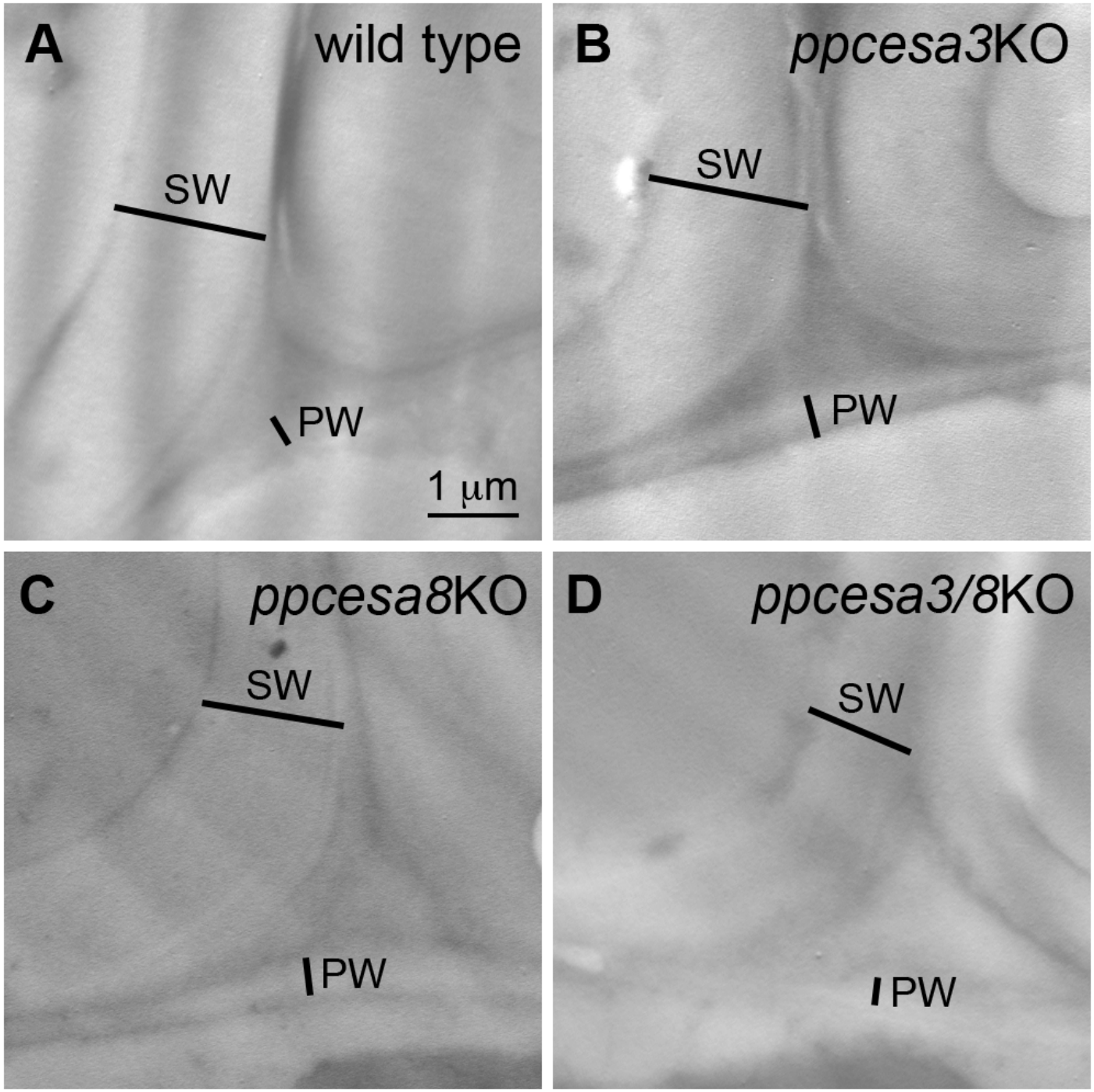

Figure 4: Transmission electron microscopy images of leaf midribs of *P. patens* showing adjacent cells with primary cell walls (PW) and secondary cell walls (SW) in (A) wild type, and (B-D) mutant leaves.

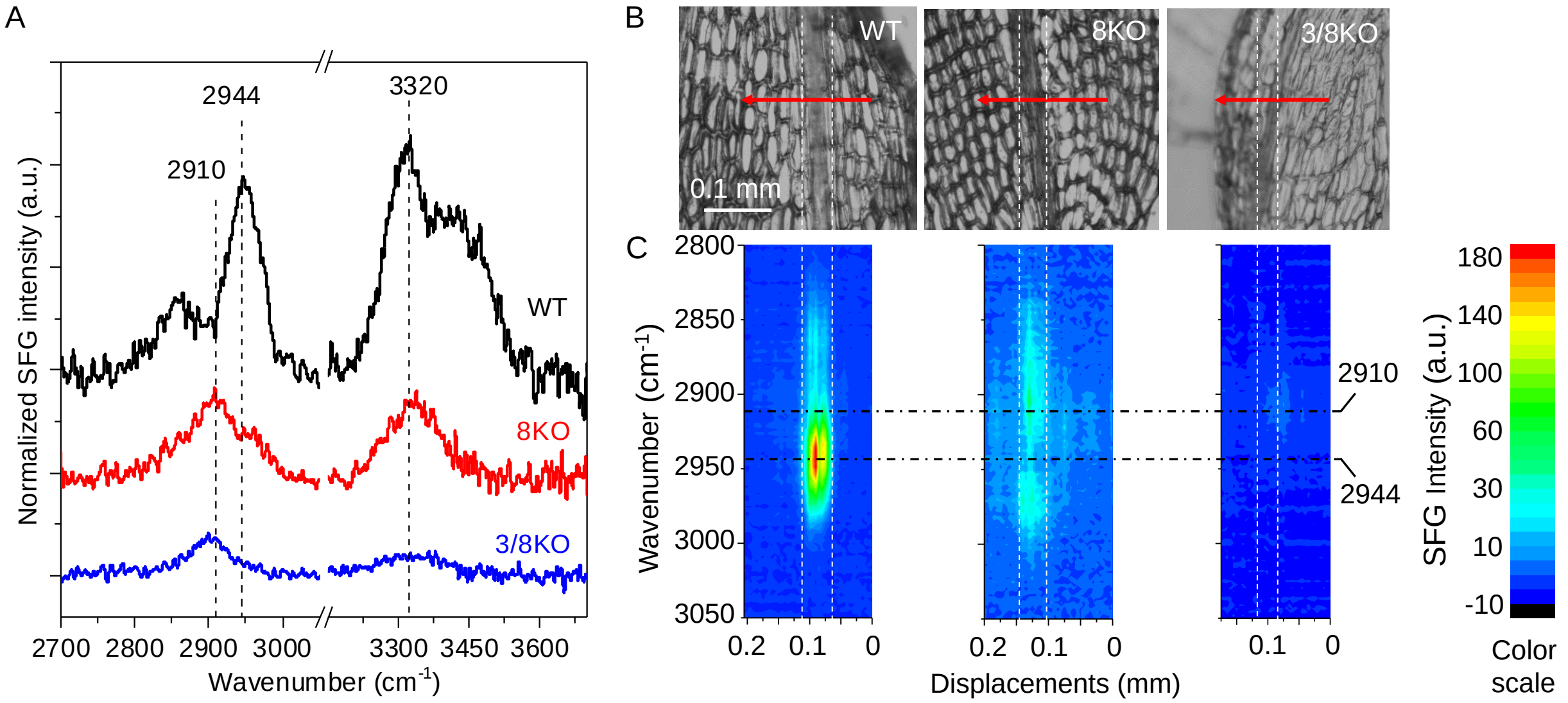

Figure 5: Sum Frequency Generation (SFG) spectroscopy of *P. patens* leaves. (A) Full SFG spectra collected from leaf midribs (each is the average of nine spectra, from three different positions on each of three different leaves). A strong peak in the C-H stretch region (2944 cm^{-1}) is present in spectra from wild type (WT), greatly diminished in spectra from *ppcesa8*KO (8KO), and absent in spectra from *ppcesa3/8*KO (3/8KO). (B) *P. patens* wild type, *ppcesa8*KO, and *ppcesa3/8*KO leaves with SFG scan trajectories traversing the midribs. Step size was 5 μm/step. SFG spectra were collected from 2850 to 3150 cm^{-1}, covering the entire CH region. (C) 2D projection image of SFG spectra collected across the midribs of each leaf shown in B. Each column in each image is an entire spectrum collected from one point, pointed against displacement along the scan trajectory. Colors indicate SFG intensity as shown in the legend.

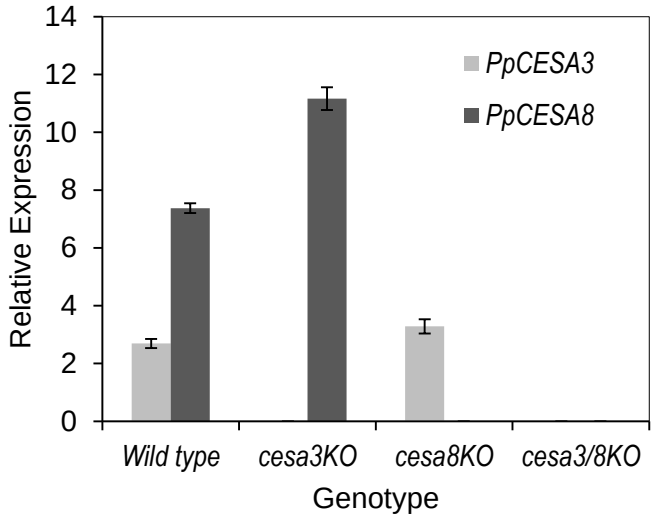

Figure 6: RT-qPCR analysis of *PpCESA3* and *PpCESA8* expression in wild type, *ppcesa3*KOs and *ppcesa8*KOs. Target/average reference cross point ratios (using actin and v-Type H^+translocating pyrophosphatase reference genes) were determined for three independent lines of each mutant (3KO-5, -35, -126; 8KO-5B, -4C, -10C; and 3/8KO-43, -57, -86) and two independent wild type lines (GD06 and GD11) with two technical replicates each. Bars indicate the standard error of the mean for the three mutant (n=3) or two wild type (n=2) lines.

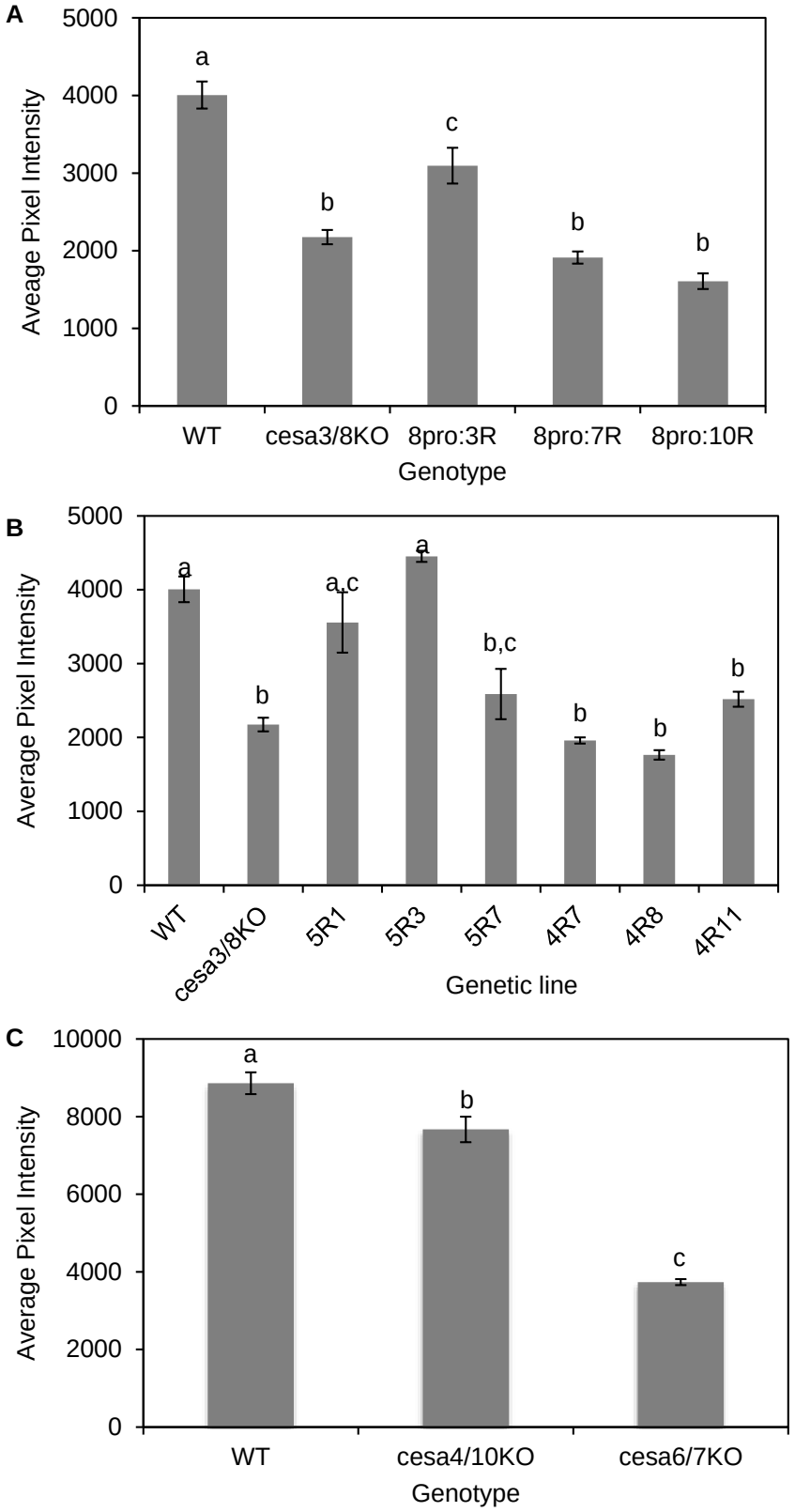

Figure 7: Quantitative analysis of S4B fluorescence intensity in leaf midribs. (A,B) Wild type (WT), *ppcesa*3/8KO-86lox, and *ppcesa*3/8KO-86lox transformed with *proCESA8::CESA* expression vectors. For each rescue genotype, three independent genetic lines were sampled in triplicate and measured with 6 samples of wild type (GD06) and 8 samples of *ppcesa*3/8KO-86lox. (A) For lines derived from transformation of *ppcesa*3/8KO-86lox with *proCESA8::CESA3* (8pro:3R), *proCESA8::CESA7* (pro8:7R), and *proCESA8::CESA10* (pro8:10R) genotypes, the three independent lines did not differ significantly and were combined. *proCESA8::CESA7* and *proCESA8::CESA10* lines did not differ significantly from the parent double KO line ($p > 0.05$), whereas *proCESA8::CESA3* lines had significantly higher fluorescence compared to the parent double KO line, but significantly less than WT ($p < 0.05$). Bars indicate the standard error of the mean for three independent lines. Genotypes with different letters are significantly different. (B) For lines derived from transformation of *ppcesa*3/8KO-86lox with *proCESA8::CESA5* (pro8:5R) and *proCESA8::CESA4* (pro8:4R), the three independent lines were significantly different and were analyzed separately. *proCESA8::CESA5* (5R) lines were not significantly different from the wild type ($p > 0.05$), except for 5R7, which was not significantly different from *ppcesa*3/8KO-86lox ($p > 0.05$). *proCESA8::CESA5* lines did not differ significantly from *ppcesa*3/8KO-86lox ($p > 0.05$). Bars indicate the standard error of the mean for three gametophores from the same line (n=3). Lines with different letters are significantly different ($p < 0.05$. (C) Mid rib fluorescence was slightly, but significantly reduced in *cesa4/10*KO compared to wild type ($p = 0.037$). Reduction in midrib fluorescence in *cesa6/7*KO was substantial and highly significant ($p = 0.0011$). Bars indicate the standard error of the mean for three independent mutant lines or 3 replicates of wild type (n=3).

Parsed Citations

Albalasmeh AA, Berhe AA, Ghezzehei TA (2013) A new method for rapid determination of carbohydrate and total carbon concentrations using UV spectrophotometry. Carbohydr Polym 97: 253-261
Pubmed: Author and Title
CrossRef: Author and Title
Google Scholar: Author Only Title Only Author and Title

Anderson CT, Carroll A, Akhmetova L, Somerville C (2010) Real-time imaging of cellulose reorientation during cell wall expansion in Arabidopsis roots. Plant Physiol 152: 787-796
Pubmed: Author and Title
CrossRef: Author and Title
Google Scholar: Author Only Title Only Author and Title

Barnett JR, Bonham VA (2004) Cellulose microfibril angle in the cell wall of wood fibres. Biol Rev Camb Philos Soc 79: 461-472
Pubmed: Author and Title
CrossRef: Author and Title
Google Scholar: Author Only Title Only Author and Title

Barnette AL, Bradley LC, Veres BD, Schreiner EP, Park YB, Park J, Park S, Kim SH (2011) Selective detection of crystalline cellulose in plant cell walls with sum-frequency-generation (SFG) vibration spectroscopy. Biomacromolecules 12: 2434-2439
Pubmed: Author and Title
CrossRef: Author and Title
Google Scholar: Author Only Title Only Author and Title

Barnette AL, Lee C, Bradley LC, Schreiner EP, Park YB, Shin H, Cosgrove DJ, Park S, Kim SH (2012) Quantification of crystalline cellulose in lignocellulosic biomass using sum frequency generation (SFG) vibration spectroscopy and comparison with other analytical methods. Carbohydr Polym 89: 802-809
Pubmed: Author and Title
CrossRef: Author and Title
Google Scholar: Author Only Title Only Author and Title

Berry EA, Tran ML, Dimos CS, Budziszek MJ, Jr., Scavuzzo-Duggan TR, Roberts AW (2016) Immuno and affinity cytochemical analysis of cell wall composition in the moss Physcomitrella patens. Front Plant Sci 7: 248
Pubmed: Author and Title
CrossRef: Author and Title
Google Scholar: Author Only Title Only Author and Title

Betancur L, Singh B, Rapp RA, Wendel JF, Marks MD, Roberts AW, Haigler CH (2011) Phylogenetically distinct cellulose synthase genes support secondary wall thickening in arabidopsis shoot trichomes and cotton fiber. J Integr Plant Biol 52: 205-220
Pubmed: Author and Title
CrossRef: Author and Title
Google Scholar: Author Only Title Only Author and Title

Blake AW, McCartney L, Flint JE, Bolam DN, Boraston AB, Gilbert HJ, Knox JP (2006) Understanding the biological rationale for the diversity of cellulose-directed carbohydrate-binding modules in prokaryotic enzymes. J Biol Chem 281: 29321-29329
Pubmed: Author and Title
CrossRef: Author and Title
Google Scholar: Author Only Title Only Author and Title

Carafa A, Duckett JG, Knox JP, Ligrone R (2005) Distribution of cell-wall xylans in bryophytes and tracheophytes: new insights into basal interrelationships of land plants. New Phytol 168: 231-240
Pubmed: Author and Title
CrossRef: Author and Title
Google Scholar: Author Only Title Only Author and Title

Carpita N, McCann M (2000) The cell wall. In: Buchanan B, Gruissem W, Jones R (eds) Biochemistry and Molecular Biology of Plants. American Society of Plant Physiologists, Rockville, MD, pp 52-108
Pubmed: Author and Title
CrossRef: Author and Title
Google Scholar: Author Only Title Only Author and Title

Carroll A, Mansoori N, Li S, Lei L, Vernhettes S, Visser RG, Somerville C, Gu Y, Trindade LM (2012) Complexes with mixed primary and secondary cellulose synthases are functional in Arabidopsis plants. Plant Physiol 160: 726-737
Pubmed: Author and Title
CrossRef: Author and Title
Google Scholar: Author Only Title Only Author and Title

Delmer DP (1999) Cellulose biosynthesis: Exciting times for a difficult field of study. Annu Rev Plant Physiol Plant Mol Biol 50: 245-276
Pubmed: Author and Title
CrossRef: Author and Title
Google Scholar: Author Only Title Only Author and Title

Desprez T, Juraniec M, Crowell EF, Jouy H, Pochylova Z, Parcy F, Hofte H, Gonneau M, Vernhettes S (2007) Organization of cellulose

synthase complexes involved in primary cell wall synthesis in Arabidopsis thaliana. Proc. Natl. Acad. Sci. USA 104: 15572-15577
Pubmed: Author and Title
CrossRef: Author and Title
Google Scholar: Author Only Title Only Author and Title

Donaldson L (2007) Cellulose microfibril aggregates and their size variation with cell wall type. Wood Sci Technol 41: 443-460
Pubmed: Author and Title
CrossRef: Author and Title
Google Scholar: Author Only Title Only Author and Title

Emons AMC, Mulder BM (2000) How the deposition of cellulose microfibrils builds cell wall architecture. Trends Plant Sci 35-40
Pubmed: Author and Title
CrossRef: Author and Title
Google Scholar: Author Only Title Only Author and Title

Fernandes AN, Thomas LH, Altaner CM, Callow P, Forsyth VT, Apperley DC, Kennedy CJ, Jarvis MC (2011) Nanostructure of cellulose microfibrils in spruce wood. Proc Natl Acad Sci U S A 108: E1195-1203
Pubmed: Author and Title
CrossRef: Author and Title
Google Scholar: Author Only Title Only Author and Title

Gonneau M, Desprez T, Guillot A, Vernhettes S, Hofte H (2014) Catalytic subunit stoichiometry within the cellulose synthase complex. Plant Physiol 166: 1709-1712
Pubmed: Author and Title
CrossRef: Author and Title
Google Scholar: Author Only Title Only Author and Title

Goss CA, Brockmann DJ, Bushoven JT, Roberts AW (2012) A CELLULOSE SYNTHASE (CESA) gene essential for gametophore morphogenesis in the moss Physcomitrella patens. Planta 235: 1355-1367
Pubmed: Author and Title
CrossRef: Author and Title
Google Scholar: Author Only Title Only Author and Title

Haigler CH, Betancur L, Stiff MR, Tuttle JR (2012) Cotton fiber: a powerful single-cell model for cell wall and cellulose research. Front Plant Sci 3: 104
Pubmed: Author and Title
CrossRef: Author and Title
Google Scholar: Author Only Title Only Author and Title

Hebant C (1977) The Conducting Tissues of Bryophytes. J. Cramer, Vaduz
Pubmed: Author and Title
CrossRef: Author and Title
Google Scholar: Author Only Title Only Author and Title

Hill JL, Jr., Hammudi MB, Tien M (2014) The Arabidopsis cellulose synthase complex: a proposed hexamer of CESA trimers in an equimolar stoichiometry. Plant Cell 26: 4834-4842
Pubmed: Author and Title
CrossRef: Author and Title
Google Scholar: Author Only Title Only Author and Title

Jarvis MC (2013) Cellulose biosynthesis: counting the chains. Plant Physiol 163: 1485-1486
Pubmed: Author and Title
CrossRef: Author and Title
Google Scholar: Author Only Title Only Author and Title

Kenrick P, Crane PR (1997) The origin and early evolution of plants on land. Nature 389: 33-39
Pubmed: Author and Title
CrossRef: Author and Title
Google Scholar: Author Only Title Only Author and Title

Kimura S, Laosinchai W, Itoh T, Cui X, Linder CR, Brown RM, Jr. (1999) Immunogold labeling of rosette terminal cellulose-synthesizing complexes in the vascular plant Vigna angularis. Plant Cell 11: 2075-2085
Pubmed: Author and Title
CrossRef: Author and Title
Google Scholar: Author Only Title Only Author and Title

Kulkarni AR, Peña MJ, Avci U, Mazumder K, Urbanowicz BR, Pattathil S, Yin Y, O'Neill MA, Roberts AW, Hahn MG, Xu Y, Darvill AG, York WS (2012) The ability of land plants to synthesize glucuronoxylans predates the evolution of tracheophytes. Glycobiology 22: 439-451
Pubmed: Author and Title
CrossRef: Author and Title
Google Scholar: Author Only Title Only Author and Title

Kumar M, Atanassov I, Turner S (2016) Functional analysis of cellulose synthase CESA protein class-specificity. Plant Physiol 173: 970-983
Pubmed: Author and Title

CrossRef: Author and Title
Google Scholar: Author Only Title Only Author and Title

Le Bail A, Scholz S, Kost B (2013) Evaluation of reference genes for RT qPCR analyses of structure-specific and hormone regulated gene expression in Physcomitrella patens gametophytes. PLoS One 8: e70998
Pubmed: Author and Title
CrossRef: Author and Title
Google Scholar: Author Only Title Only Author and Title

Lee CM, Kafle K, Huang S, Kim SH (2016) Multimodal Broadband Vibrational Sum Frequency Generation (MM-BB-V-SFG) Spectrometer and Microscope. J Phys Chem B 120: 102-116
Pubmed: Author and Title
CrossRef: Author and Title
Google Scholar: Author Only Title Only Author and Title

Lee CM, Kafle K, Park YB, Kim SH (2014) Probing crystal structure and mesoscale assembly of cellulose microfibrils in plant cell walls, tunicate tests, and bacterial films using vibrational sum frequency generation (SFG) spectroscopy. Phys Chem Chem Phys 16: 10844-10853
Pubmed: Author and Title
CrossRef: Author and Title
Google Scholar: Author Only Title Only Author and Title

Ligrone R, Vaughn KC, Renzaglia KS, Knox JP, Duckett JG (2002) Diversity in the distribution of polysaccharide and glycoprotein epitopes in the cell walls of bryophytes: new evidence for the multiple evolution of water-conducting cells. New Phytol 156: 491-508
Pubmed: Author and Title
CrossRef: Author and Title
Google Scholar: Author Only Title Only Author and Title

Lindeboom J, Mulder BM, Vos JW, Ketelaar T, Emons AM (2008) Cellulose microfibril deposition: coordinated activity at the plant plasma membrane. J Microsc 231: 192-200
Pubmed: Author and Title
CrossRef: Author and Title
Google Scholar: Author Only Title Only Author and Title

Newman RH, Hill SJ, Harris PJ (2013) Wide-angle x-ray scattering and solid-state nuclear magnetic resonance data combined to test models for cellulose microfibrils in mung bean cell walls. Plant Physiol 163: 1558-1567
Pubmed: Author and Title
CrossRef: Author and Title
Google Scholar: Author Only Title Only Author and Title

Nixon BT, Mansouri K, Singh A, Du J, Davis JK, Lee JG, Slabaugh E, Vandavasi VG, O'Neill H, Roberts EM, Roberts AW, Yingling YG, Haigler CH (2016) Comparative structural and computational analysis supports eighteen cellulose synthases in the plant cellulose synthesis complex. Sci Rep 6: 28696
Pubmed: Author and Title
CrossRef: Author and Title
Google Scholar: Author Only Title Only Author and Title

Oehme DP, Downton MT, Doblin MS, Wagner J, Gidley MJ, Bacic A (2015) Unique aspects of the structure and dynamics of elementary Ibeta cellulose microfibrils revealed by computational simulations. Plant Physiol 168: 3-17
Pubmed: Author and Title
CrossRef: Author and Title
Google Scholar: Author Only Title Only Author and Title

Park YB, Lee CM, Koo BW, Park S, Cosgrove DJ, Kim SH (2013) Monitoring meso-scale ordering of cellulose in intact plant cell walls using sum frequency generation spectroscopy. Plant Physiol 163: 907-913
Pubmed: Author and Title
CrossRef: Author and Title
Google Scholar: Author Only Title Only Author and Title

Persson S, Paredez A, Carroll A, Palsdottir H, Doblin M, Poindexter P, Khitrov N, Auer M, Somerville CR (2007) Genetic evidence for three unique components in primary cell-wall cellulose synthase complexes in Arabidopsis. Proc. Natl. Acad. Sci. USA 104: 15566-15571
Pubmed: Author and Title
CrossRef: Author and Title
Google Scholar: Author Only Title Only Author and Title

Rensing SA, Lang D, Zimmer AD, Terry A, Salamov A, Shapiro H, Nishiyama T, Perroud PF, Lindquist EA, Kamisugi Y, Tanahashi T, Sakakibara K, Fujita T, Oishi K, Shin IT, Kuroki Y, Toyoda A, Suzuki Y, Hashimoto S, Yamaguchi K, Sugano S, Kohara Y, Fujiyama A, Anterola A, Aoki S, Ashton N, Barbazuk WB, Barker E, Bennetzen JL, Blankenship R, Cho SH, Dutcher SK, Estelle M, Fawcett JA, Gundlach H, Hanada K, Heyl A, Hicks KA, Hughes J, Lohr M, Mayer K, Melkozernov A, Murata T, Nelson DR, Pils B, Prigge M, Reiss B, Renner T, Rombauts S, Rushton PJ, Sanderfoot A, Schween G, Shiu SH, Stueber K, Theodoulou FL, Tu H, Van de Peer Y, Verrier PJ, Waters E, Wood A, Yang L, Cove D, Cuming AC, Hasebe M, Lucas S, Mishler BD, Reski R, Grigoriev IV, Quatrano RS, Boore JL (2008) The Physcomitrella genome reveals evolutionary insights into the conquest of land by plants. Science 319: 64-69
Pubmed: Author and Title
CrossRef: Author and Title
Google Scholar: Author Only Title Only Author and Title

Roberts AW, Bushoven JT (2007) The cellulose synthase (CESA) gene superfamily of the moss Physcomitrella patens. Plant Mol Biol 63: 207-219
Pubmed: Author and Title
CrossRef: Author and Title
Google Scholar: Author Only Title Only Author and Title

Roberts AW, Dimos C, Budziszek MJ, Goss CA, Lai V (2011) Knocking out the wall: protocols for gene targeting in Physcomitrella patens. Methods Mol Biol 715: 273-290
Pubmed: Author and Title
CrossRef: Author and Title
Google Scholar: Author Only Title Only Author and Title

Roberts AW, Roberts EM, Haigler CH (2012) Moss cell walls: structure and biosynthesis. Front Plant Sci 3: 166
Pubmed: Author and Title
CrossRef: Author and Title
Google Scholar: Author Only Title Only Author and Title

Scavuzzo-Duggan TR, Chaves AM, Roberts AW (2015) A complementation assay for in vivo protein structure/function analysis in Physcomitrella patens (Funariaceae). App Plant Sci 3: 1500023
Pubmed: Author and Title
CrossRef: Author and Title
Google Scholar: Author Only Title Only Author and Title

Schaefer DG, Zryd JP (1997) Efficient gene targeting in the moss Physcomitrella patens. Plant J 11: 1195-1206
Pubmed: Author and Title
CrossRef: Author and Title
Google Scholar: Author Only Title Only Author and Title

Schindelin J, Arganda-Carreras I, Frise E, Kaynig V, Longair M, Pietzsch T, Preibisch S, Rueden C, Saalfeld S, Schmid B, Tinevez JY, White DJ, Hartenstein V, Eliceiri K, Tomancak P, Cardona A (2012) Fiji: an open-source platform for biological-image analysis. Nat Methods 9: 676-682
Pubmed: Author and Title
CrossRef: Author and Title
Google Scholar: Author Only Title Only Author and Title

Schuetz M, Smith R, Ellis B (2013) Xylem tissue specification, patterning, and differentiation mechanisms. J Exp Bot 64: 11-31
Pubmed: Author and Title
CrossRef: Author and Title
Google Scholar: Author Only Title Only Author and Title

Shen H, Yin Y, Chen F, Xu Y, Dixon RA (2009) A bioinformatic analysis of NAC genes for plant cell wall development in relation to lignocellulosic bioenergy production. Bioenerg Res 2: 217-232
Pubmed: Author and Title
CrossRef: Author and Title
Google Scholar: Author Only Title Only Author and Title

Taylor JG, Owen TP, Jr., Koonce LT, Haigler CH (1992) Dispersed lignin in tracheary elements treated with cellulose synthesis inhibitors provides evidence that molecules of the secondary cell wall mediate wall patterning. Plant J 2: 959-970
Pubmed: Author and Title
CrossRef: Author and Title
Google Scholar: Author Only Title Only Author and Title

Taylor NG, Gardiner JC, Whiteman R, Turner SR (2004) Cellulose synthesis in the Arabidopsis secondary cell wall. Cellulose 11: 329-338
Pubmed: Author and Title
CrossRef: Author and Title
Google Scholar: Author Only Title Only Author and Title

Taylor NG, Howells RM, Huttly AK, Vickers K, Turner SR (2003) Interactions among three distinct CesA proteins essential for cellulose synthesis. Proc Natl Acad Sci USA 100: 1450-1455
Pubmed: Author and Title
CrossRef: Author and Title
Google Scholar: Author Only Title Only Author and Title

Taylor NG, Laurie S, Turner SR (2000) Multiple cellulose synthase catalytic subunits are required for cellulose synthesis in Arabidopsis. Plant Cell 12: 2529-2539
Pubmed: Author and Title
CrossRef: Author and Title
Google Scholar: Author Only Title Only Author and Title

Thomas LH, Forsyth VT, Martel A, Grillo I, Altaner CM, Jarvis MC (2014) Structure and spacing of cellulose microfibrils in woody cell walls of dicots. Cellulose 21: 3887-3895
Pubmed: Author and Title
CrossRef: Author and Title
Google Scholar: Author Only Title Only Author and Title

Timmers J, Vernhettes S, Desprez T, Vincken JP, Visser RG, Trindade LM (2009) Interactions between membrane-bound cellulose synthases involved in the synthesis of the secondary cell wall. FEBS Lett. 583: 978-982
Pubmed: Author and Title
CrossRef: Author and Title
Google Scholar: Author Only Title Only Author and Title

Tran ML, Roberts AW (2016) Cellulose synthase (CESA) gene expression profiling of Physcomitrella patens. . Plant Biol 18: 362-368
Pubmed: Author and Title
CrossRef: Author and Title
Google Scholar: Author Only Title Only Author and Title

Updegraff DM (1969) Semimicro determination of cellulose in biological materials. Anal Biochem 32: 420-424
Pubmed: Author and Title
CrossRef: Author and Title
Google Scholar: Author Only Title Only Author and Title

Vandavasi VG, Putnam DK, Zhang Q, Petridis L, Heller WT, Nixon BT, Haigler CH, Kalluri U, Coates L, Langan P, Smith JC, Meiler J, O'Neill H (2016) A structural study of CESA1 catalytic domain of Arabidopsis cellulose synthesis complex: evidence for CESA trimers. Plant Physiol 170: 123-135
Pubmed: Author and Title
CrossRef: Author and Title
Google Scholar: Author Only Title Only Author and Title

Vidali L, Burkart GM, Augustine RC, Kerdavid E, Tuzel E, Bezanilla M (2010) Myosin XI is essential for tip growth in Physcomitrella patens. Plant Cell 22: 1868-1882
Pubmed: Author and Title
CrossRef: Author and Title
Google Scholar: Author Only Title Only Author and Title

Vidali L, van Gisbergen PA, Guerin C, Franco P, Li M, Burkart GM, Augustine RC, Blanchoin L, Bezanilla M (2009) Rapid formin-mediated actin-filament elongation is essential for polarized plant cell growth. Proc Natl Acad Sci U S A 106: 13341-13346
Pubmed: Author and Title
CrossRef: Author and Title
Google Scholar: Author Only Title Only Author and Title

Wilson SM, Bacic A (2012) Preparation of plant cells for transmission electron microscopy to optimize immunogold labeling of carbohydrate and protein epitopes. Nat Protoc 7: 1716-1727
Pubmed: Author and Title
CrossRef: Author and Title
Google Scholar: Author Only Title Only Author and Title

Wise HZ, Saxena IM, Brown RM, Jr. (2011) Isolation and characterization of the cellulose synthase genes PpCesA6 and PpCesA7 in Physcomitrella patens. Cellulose 18: 371-384
Pubmed: Author and Title
CrossRef: Author and Title
Google Scholar: Author Only Title Only Author and Title

Xu B, Ohtani M, Yamaguchi M, Toyooka K, Wakazaki M, Sato M, Kubo M, Nakano Y, Sano R, Hiwatashi Y, Murata T, Kurata T, Yoneda A, Kato K, Hasebe M, Demura T (2014) Contribution of NAC transcription factors to plant adaptation to land. Science 343: 1505-1508
Pubmed: Author and Title
CrossRef: Author and Title
Google Scholar: Author Only Title Only Author and Title

Yang JH, Wang H (2016) Molecular mechanisms for vascular development and secondary cell wall formation. Front Plant Sci 7: 356
Pubmed: Author and Title
CrossRef: Author and Title
Google Scholar: Author Only Title Only Author and Title

Yin Y, Huang J, Xu Y (2009) The cellulose synthase superfamily in fully sequenced plants and algae. BMC Plant Biol 9: 99
Pubmed: Author and Title
CrossRef: Author and Title
Google Scholar: Author Only Title Only Author and Title

Zhong R, Ye ZH (2015) Secondary cell walls: biosynthesis, patterned deposition and transcriptional regulation. Plant Cell Physiol 56: 195-214
Pubmed: Author and Title
CrossRef: Author and Title
Google Scholar: Author Only Title Only Author and Title

Zhu T, Nevo E, Sun D, Peng J (2012) Phylogenetic analyses unravel the evolutionary history of NAC proteins in plants. Evolution 66: 1833-1848
Pubmed: Author and Title
CrossRef: Author and Title
Google Scholar: Author Only Title Only Author and Title